



Netherlands Enterprise Agency

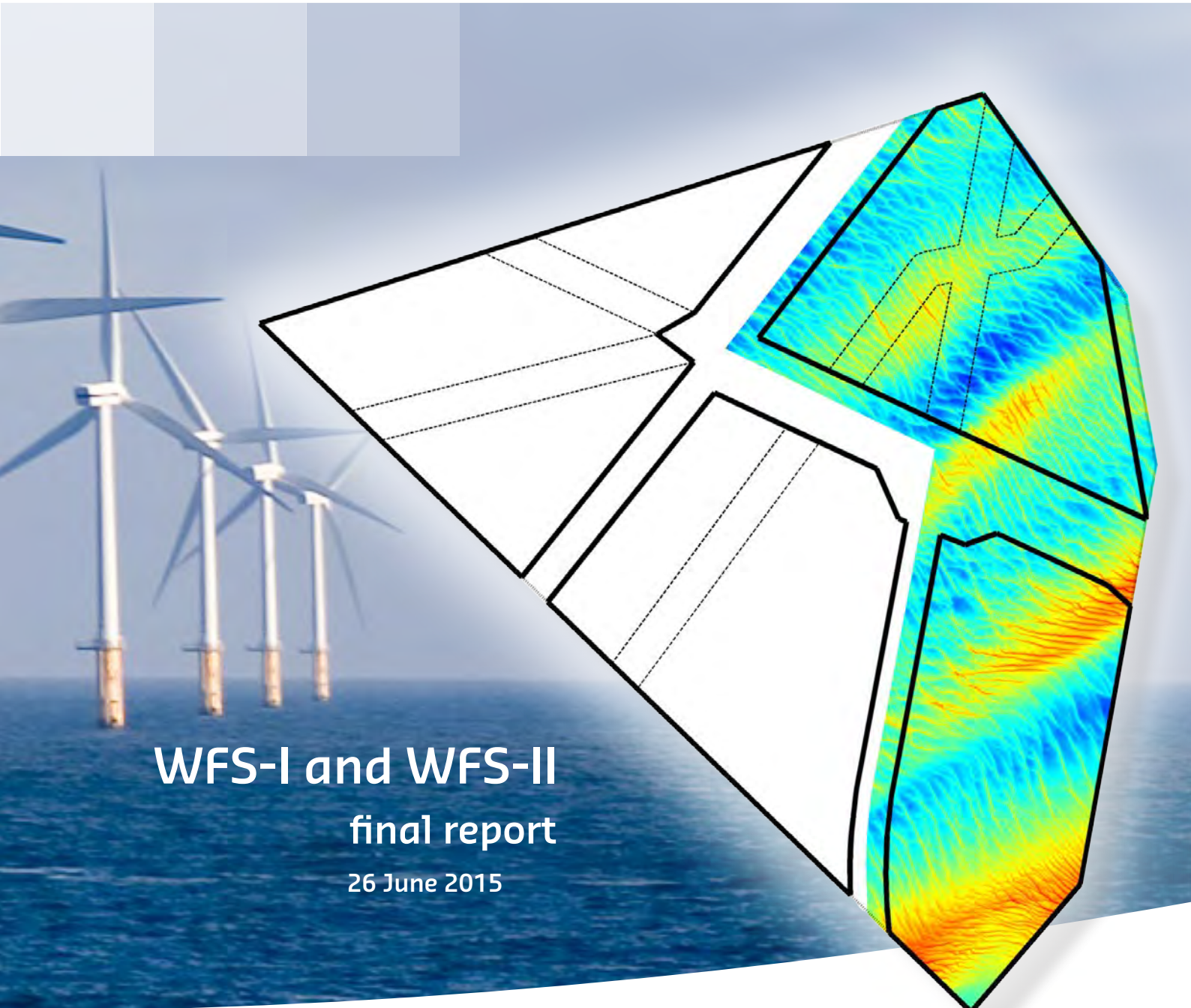
Morphodynamics of Borssele Wind Farm Zone WFS-I and WFS-II Final Report

Prediction of seabed level changes between 2015 and 2046

*>> Sustainable. Agricultural. Innovative.
International.*



Morphodynamics of Borssele Wind Farm Zone



WFS-I and WFS-II

final report

26 June 2015

Netherlands Enterprise Agency (RVO.nl)
Croeselaan 15 | 3521 BJ | Utrecht
P.O. Box 8242 | 3503 RE | Utrecht
Netherlands

Det Norske Veritas, Danmark A/S
DNV GL Energy
Technical
Tuborg Parkvej 8, 2nd Floor
DK2900 Hellerup
-
Denmark
Tel: +45 39 45 48 00
Fax: +45 39 45 48 01

Date: 2015-07-15
Our reference: DNV Doc. No:1KI2TUA-9
Sign:EAH
Corresp. No.:

Your reference:

Zone Borssele Site Data

DNV GL has reviewed the Deltares report
Morphodynamics of Borssele Wind Farm Zone WFS-I and WFS-II. Prediction of seabed level changes between 2015 and 2046. Doc. no.: 1210520-000 final version issued 2015-06-26.

DNV GL has found that

- 1) the Reference Seabed Levels (RSBLs) presented in figure 5.5 and
- 2) the Maximum Seabed Level (MSBLs) presented in figure 5.7

obtained by surveys carried out in the period from 1999 to 2015, are determined according to best engineering practices. The maps indicate correctly, the respectively potentially lowest and highest seabed levels for future offshore wind farms in the Borssele Wind Farm Zone WFS-I and WFS-II.

Sincerely
for Det Norske Veritas, Danmark A/S

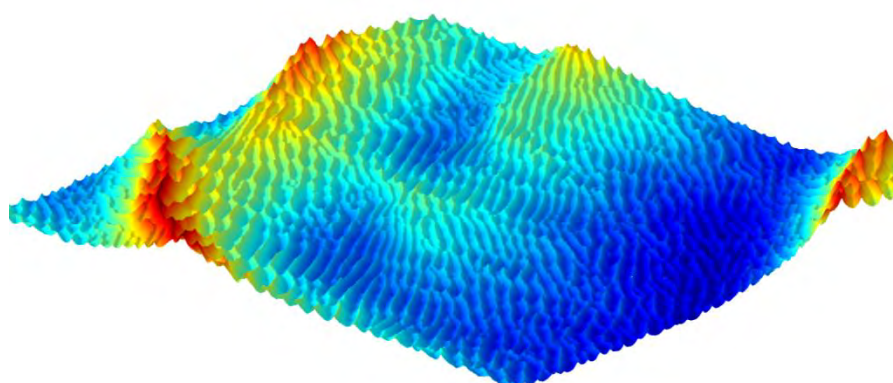
For: 
Erik Asp Hansen
Project Manager & Principal Engineer
Mobile: +45 20 27 38 71
Direct: +45 39 45 48 71
erik.asp.hansen@dnvgl.com


Lohmann, Iris Pernille
2015.07.15 10:41:49
+02'00'
Iris Lohmann
Senior Engineer
Mobile: +45 60 35 15 56
Direct: +45 39 45 49 53
iris.lohmann@dnvgl.com

Morphodynamics of Borssele Wind Farm Zone WFS-I and WFS-II - final report

prediction of seabed level changes between 2015 and 2046

Robert Hasselaar
Tim Raaijmakers
Hendrik Jan Riezebos
Thaiënne van Dijk
Bas Borsje
Tommer Vermaas



1210520-000

Title

Morphodynamics of Borssele Wind Farm Zone
WFS-I and WFS-II - final report

Client

Rijksdienst voor
Ondernemend Nederland

Project

1210520-000

Reference

1210520-000-HYE-0004

Keywords

Seabed morphodynamics, offshore wind, Borssele, sand waves, bed form migration

Summary

This report is the result of the second phase of the morphodynamic analysis of the Borssele Wind Farm Zone (BWFZ). In this phase, the results of phase I were updated on the basis of a new survey that was performed early 2015. The BWFZ is located just north of the Dutch-Belgian border and is sub-divided into four sites with a combined area of approximately 234km². The morphology of the system is classified as highly dynamic, with a complex bathymetry consisting of static (in the timespan between 2000 and 2015), shore-parallel sandbanks overlain with dynamic shore-perpendicular sand waves. Within the area, opposing migration directions for the sand waves were found with sand going towards SW-direction and to the opposing NE-direction (with a variation of up to 30° in both directions).

In this report, sand wave characteristics were determined for the combined area of WFS-1 and WFS-II as well as for the individual sites by means of consistent tracking of crest and trough points of individual sand waves from various transects of 1750 meter, equally distributed throughout the BWFZ. The sand waves in WFS-I and WFS-II have a wavelength between 130 and 430 meters, a wave height between 1.9 and 5.9 meters and migration speeds in the order of -1.7m/yr (in NE-direction) to 1.9 m/yr (in the governing SW-direction).

Next, the reference seabed level (RSBL) and maximum seabed level (MSBL) were determined, indicating the predicted lowest and highest seabed levels during the lifetime of the wind farms in the Borssele area. Comparison of the RSBL with the most recent bathymetry from 2015 showed a potential maximum local lowering of the seabed of approximately 5m. A comparison of the RSBL with the base of the Holocene Formation showed that no unrealistic values for the seabed lowering were computed in this study.

The predicted seabed level changes presented in this study follow from the applied morphological analysis techniques, describing the (uncertainty of the) physics and the natural variability of the analysed morphological system. No additional safety margins for design purposes have been applied.

Copyright © Staat der Nederlanden, 2015. All rights reserved.

The contents of this report were developed by Stichting Deltares, specifically at the request of the Ministry of Economic Affairs. No warranty of any kind, for any particular purpose, is provided or implied with respect to the contents of this report. Use of the information contained in this report is at the sole expense and risk of the person or entity doing so. Deltares disclaims any and all liability for any loss or damage suffered as a result of using the information published in this report.

References

Request for Offer: RVO, SDE1400015, registration number IUC/201408261500, dated 1 September 2014.

Proposal: Deltares, 1210520-000-HYE-0001-o-Quotation for Morphodynamical and Geomorphological Conditions of the Borssele Wind Zone, dated 12 September 2014.

Contract award: RVO, SDE1400015, registration number IUC/201408261500, dated 22 September 2014.

Report first phase: Deltares, 1210520-000-HYE-0002, Morphodynamics of Borssele Wind Farm Zone, prediction of potential seabed level changes during the lifetime of offshore wind parks, dated 23 December 2014.

Version	Date	Author	Initials	Review	Initials	Approval	Initials
Draft	10 June 2015	Robert Hasselaar		Dirk-Jan Walstra		KlaasJan Bos	
		Tim Raaijmakers					
		Hendrik Jan Riezebos					
Final	26 June 2015	Bas Borsje		Dirk-Jan Walstra		KlaasJan Bos	
		Thaiënne van Dijk					
		Tommer Vermaas					

State
final

Contents

Samenvatting (<i>in Dutch</i>)	2
1 Introduction	3
1.1 Background	3
1.2 Objectives	3
1.3 Contents of report	4
2 Description of available data, seabed features and project area	5
2.1 Introduction	5
2.2 Available datasets by Netherlands Hydrographic Office	5
2.3 New dataset by Deep in 2015	6
2.4 Geodetic parameters	7
2.5 Generic characterization of morphodynamic seabed features	8
2.6 Background information on sand waves and their physical processes	9
2.7 Characterization of Borssele Wind Farm Zone	13
3 Data analysis and pre-processing for sand wave analysis	17
3.1 Introduction to methodology	17
3.2 Large-scale bathymetric filtering	19
3.3 Analysis of megaripples	22
3.4 Resulting sand wave field for sand wave analysis	25
4 Sand wave analysis	26
4.1 Introduction	26
4.2 Determination of directions of sand wave migration	26
4.3 Fourier analysis on individual bed forms	29
4.3.1 Sand wave statistics of the Borssele wind farm zone	32
4.3.2 Sand wave statistics per site	39
5 Prediction of future bathymetries and bed level changes	41
5.1 Introduction	41
5.2 Sources for uncertainty	41
5.3 Predicting future bathymetries and bed level changes in period 2015-2046	44
5.4 Reference SeaBed Level (RSBL)	47
5.5 Maximum SeaBed Level (MSBL)	49
5.6 Comparison of RSBL with base of Holocene formations	51
5.7 Classification zones for offshore foundations and cables	55
6 Conclusions and recommendations	58
6.1 Conclusions	58
6.2 Recommendations	59
References	60

Samenvatting (*in Dutch*)

De Rijksdienst voor Ondernemend Nederland (RVO) heeft Deltares opdracht gegeven om een morfodynamische analyse uit te voeren voor het nieuwe windenergiegebied Borssele (BWFZ = Borssele Wind Farm Zone) aan de zuidzijde van de Nederlandse Exclusieve Economische Zone. Het gehele gebied bestaat uit 4 kavels en beslaat een oppervlak van ca. 234 km². Dit rapport beschrijft de tweede fase van de morfodynamische analyse, waarin de recente bodem-surveys van kavels I en II (Deep, 2015a, 2015b) zijn gebruikt om de eerdere resultaten (Deltares, 2014) te verfijnen.

Het doel van de morfodynamische analyse is om de verschillende bodemvormen in kaart te brengen en de mogelijke bodemveranderingen in de periode 2015-2046 te kwantificeren, zowel in opwaartse als neerwaartse richting. Met deze resultaten kunnen de windparkontwikkelaars vervolgens de ondersteuningsconstructies en kabeltracés ontwerpen.

De morfologie van BWFZ kan worden gekarakteriseerd als erg dynamisch met een complexe bathymetrie opgebouwd uit statische (tenminste gedurende de periode 2000-2015) zandbanken parallel aan de kust en loodrecht hierop dynamische zandgolven. In dit gebied komen zandgolven met tegengestelde migratierichting voor: sommige zandgolven migreren richting het zuidwesten, terwijl andere zandgolven zich richting het noordoosten bewegen. Variaties tot 30° op deze hoofdrichtingen treden op.

In deze studie zijn de zandgolfkarakteristieken bepaald voor kavels I en II door het automatisch en consistent volgen van de toppen en dalen van individuele zandgolven in verschillende doorsnedes van 1750m lang, evenredig verdeeld over BWFZ. De zandgolven in kavels I en II hebben een lengte van 130 tot 430m, een golfhoogte van 1.9 tot 5.9m en migratiesnelheden variërend van 1.7 m/jaar richting het noordoosten tot 1.9 m/jaar richting het zuidwesten.

Vervolgens is op basis van deze berekende zandgolfdynamiek de laagst en hoogst mogelijke zeebodempligging bepaald voor de periode 2015-2046. Deze twee bodemniveaus worden respectievelijk RSBL (Reference SeaBed Level) en MSBL (Maximum SeaBed Level) genoemd. Vergelijking van de RSBL met de huidige bathymetrie in 2015 levert een maximale potentiële bodemdaling van ongeveer 5m op voor sommige locaties. Als extra kwaliteitscontrole is het RSBL vergeleken met de basis van de Holocene Formatie (die is verkregen door metingen met een Sub Bottom Profiler). Deze vergelijking leerde dat er geen onrealistische waarden voor de bodemdaling zijn voorspeld in deze studie.

Om de geschiktheid van gebieden voor de plaatsing van ondersteuningsconstructies en elektriciteitskabels te illustreren zijn kaarten gemaakt, die het gebied classificeren in "aanbevolen", "mogelijk", "beter vermijden" en "niet aanbevolen". De precieze indeling van deze gebieden is afhankelijk van acceptabele bodemveranderingen voor de windparkontwikkelaars en dienen daarom alleen ter illustratie. Wanneer de precieze eisen bekend zijn (bijv. wanneer de ondersteuningsconstructie bekend is) kunnen deze kaarten worden aangepast.

De voorspelde bodemveranderingen volgen uit de toegepaste, state-of-the-art analysemethoden en zijn gebaseerd op de beschikbare bodemmetingen. Onzekerheden in de (nauwkeurigheid van de) bodemdata, de fysieke processen verantwoordelijk voor bodemdynamiek en de natuurlijke variatie in het systeem zijn zo goed mogelijk meegenomen in de onzekerheidsbanden. Er zijn geen additionele veiligheidsfactoren voor ontwerptoeepassingen op de resultaten toegepast.

1 Introduction

1.1 Background

The Dutch government has designated three areas in the Dutch part of the North Sea for offshore wind farm development. The first area to be developed is the Borssele Wind Farm Zone (BWFZ). This area is located just north of the Dutch-Belgian border. Several pipelines and telecom cables are crossing the BWFZ, which is sub-divided into four sites with a combined area of approximately 234km².

A first geological desk study for the Borssele Wind Farm Zone was performed by Crux Engineering BV (2014). In this study, the morphodynamic behaviour of the seabed in the BWFZ was not investigated. The morphodynamics of an offshore wind farm area however determine the design of turbine foundations and horizontal and vertical infield and export cable routes to a great extent. Therefore, RVO requested a proposal from Deltares to determine the morphological conditions of the Borssele Wind Farm Zone by letter dated 1 September 2014 (reference: SDE1400015). On 12 September 2014 the proposal was submitted by Deltares (reference: 1210520-000-HYE-0001). The project was awarded on 22 September 2014 and after signing of the contract and delivery of the data to Deltares, the project started with the first phase on 2 October 2014. In this first phase only already available bathymetric data was used. The (most recent) revised draft report of this first phase is dated 23 December 2014.

To increase the accuracy and reduce the conservatism in the values obtained in the first phase an additional dataset of bathymetric data was considered very valuable. In the original scope for Deltares a second phase was therefore already included in which the uncertainty ranges in the results of the first phase were to be reduced. In the first months of 2015 these data were obtained by Deep for the first two wind farm sites of BWFZ (WFS-I and WFS-II). The surveys of the third and fourth site are planned for the summer of 2015. This report details the updated results for WFS-I and WFS-II using the most recent 2015 bathymetry data and the 2000/2010 bathymetrical data from phase I. The predictions in this report are made for a period of 31 years from 2015-2046.

1.2 Objectives

The study by Deltares is conducted in two phases. The first phase aimed at improving the morphological understanding of the Borssele Wind Farm Zone, based on the already available (bathymetrical) information. In this second phase, the results of the first phase were updated based on the results of a field investigation of the BWFZ by DEEP in the first months of 2015.

The objectives are:

- To update and validate the findings of the first phase by means of inclusion of a new, high resolution bathymetrical dataset
- To deliver GIS-files with different "classification zones" for foundations and electricity cables (e.g. recommended, possible but with some additional measures to be taken, better to be avoided, highly un-recommended, etc.)

1.3 Contents of report

This report provides a general description of the available datasets in Chapter 2. Furthermore, this chapter provides a generic characterization of and background information on morphodynamic seabed features and a specific characterization of the BWFZ. Chapter 3 provides the description of the bathymetric data analysis and further pre-processing of the data that is required for the sand wave analysis that is discussed in the next chapter, Chapter 4. The prediction of future bathymetries and corresponding seabed level changes, relative to the 2015 bathymetry, are discussed in Chapter 5. The report finishes with conclusions and recommendations in Chapter 6.

2 Description of available data, seabed features and project area

2.1 Introduction

In this chapter the available in-house datasets are described in Section 2.2. These datasets were used in the first phase of this project. Recently, additional geophysical and bathymetrical data was recorded by Deep, which is described in Section 2.3. The coordinate system and geodetic parameters used in this study are presented in Section 2.4. Some background information on morphodynamic seabed features of various length scales is given in Section 2.5. Since sand waves are the dominant seabed feature the next section (Section 2.6) zooms in on the physical processes responsible for sand wave generation and migration. In Section 2.7 a global characterization of the project area is presented.

2.2 Available datasets by Netherlands Hydrographic Office

The project site is located outside the survey boundary of Rijkswaterstaat. Therefore, all available historical survey data were collected by the Netherlands Hydrographic Office (NLHO) of the Netherlands Royal Navy (IHO, 1988). In the area surrounding the BWFZ, a total of fourteen surveys has been conducted between 1988 and 2014. The scientific validation of this survey policy was investigated in Deltares (2011). The datasets are summarized in Table 2.1.

Year	Survey ID NLHO	Survey Method	Data density	Coverage	Used in this study
1988	7727	SBES	Low	Part of site I	No
1988	7744	SBES	Low	Part of site IV	No
1988	7745	SBES	Low	Parts of site III and IV	No
1990	7784	SBES	Low	Parts of site III and IV	No
1990	7722	SBES	Average	Part of site I	No
1999	6264	SBES	Average	Part of site II	Yes
1999	4737	SBES	Average	Part of site I, II and III	Yes
2000	6104	SBES	High	Part of site I	Yes
2001	10426	Unknown	High	Part of site II	No
2001	6544	SBES	High	Parts of site III and IV	Yes
2004	12644	Unknown	Low	Part of site II	No
2010	15235	MBES	Excellent	NE part of BWFZ	Yes
2010	15236	MBES	Excellent	Middle part of BWFZ	Yes
2010	15409	MBES	Excellent	SW part of BWFZ	Yes

Table 2.1 Overview of available surveys from the NLHO. SBES means Single Beam Echo Sounder, MBES means Multi Beam Echo Sounder.

A continuous bathymetry from the NLHO, covering the entire BWFZ-project area, is available for the 2010 situation only (see Figure 2.8). The surveys conducted in that year provide an excellent high resolution dataset. For the investigation of the temporal development of the morphology in the area, more surveys are required. Therefore, four surveys around the year 2000 are combined into one dataset. The resulting bathymetry is displayed in Figure 2.1. This implies that two datasets of the entire BWFZ-project area were derived from the NLHO data, from 2000 (combined) and 2010. Because the surveys from before 1999 do not cover the entire BWFZ and are of low resolution, these surveys are discarded.

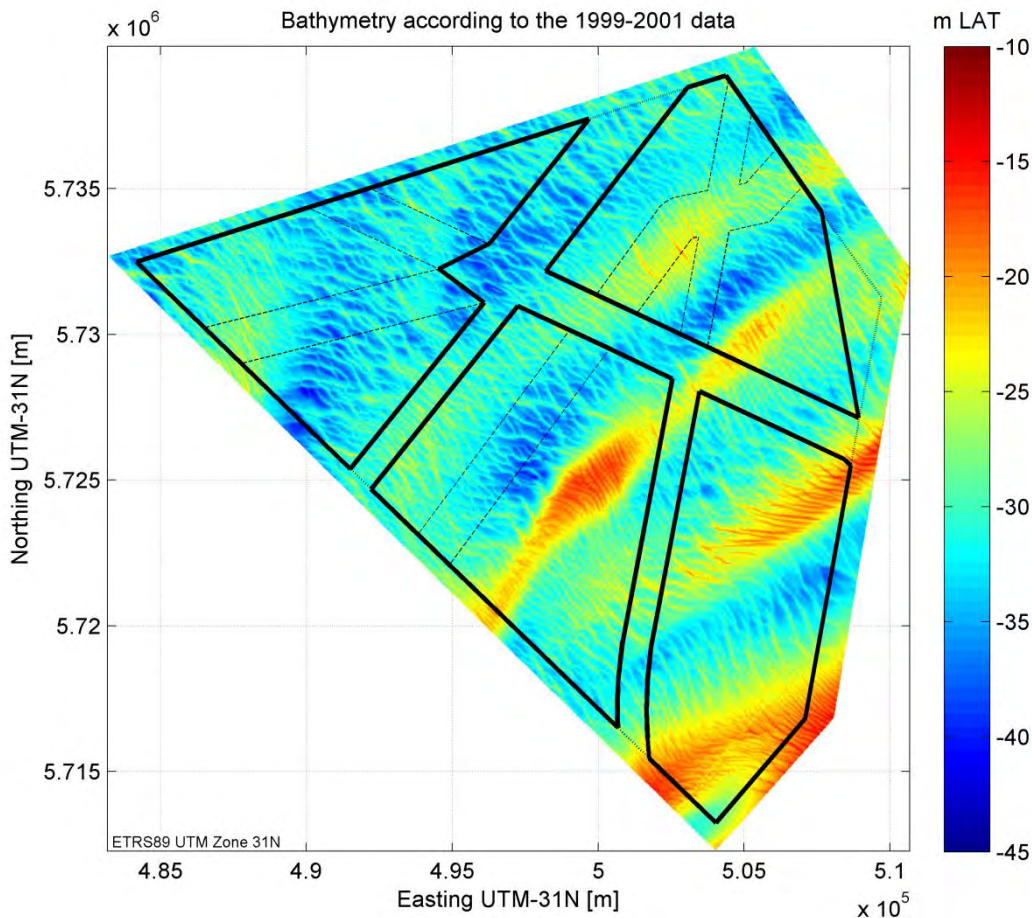


Figure 2.1 Bathymetry consisting of the combined 1999, 2000 and 2001 surveys. Bed levels are given in meters relative to Lowest Astronomical Tide (LAT).

2.3 New dataset by Deep in 2015

RVO commissioned Deep to perform a full bathymetric and geophysical survey of wind farm sites I and II. The measurement campaigns of wind farm sites III and IV are currently ongoing and the results will be delivered in the near future. Several types of surveys were conducted:

1. multi-beam survey (hereafter MBES)
2. side scan sonar (hereafter SSS)
3. sub-bottom profiler survey (hereafter SBP)
4. magnetometer survey (hereafter MAG)
5. multi-channel sparker seismic survey (MCS)

The first four surveys were obtained with vessel MV Breaker in the period between 26 January and 15 February 2015. To avoid interference from the sparker system on other survey techniques the fifth survey was performed with another vessel (MV Seazip Surveyor); these data were obtained in the period between 16 and 28 January 2015.

In this study, the multi-beam survey (1) was used to obtain an additional high quality dataset to compute the expected bed level changes for the period 2015-2046 with greater accuracy. The bathymetry is plotted in Figure 2.2. The results were compared with the isopach,

representing the base of the Holocene Formations obtained by the subsea bottom profiler (3), to check whether the computed values for the downward bed level movement were not penetrating through the base of the Holocene Formations. This step was performed to avoid overly conservative results.

Analysing data of the other surveys was not part of the scope of this study. This means for instance that detected ship wrecks and their influence on local morphodynamics (e.g. local scour) are not considered in the analysis.

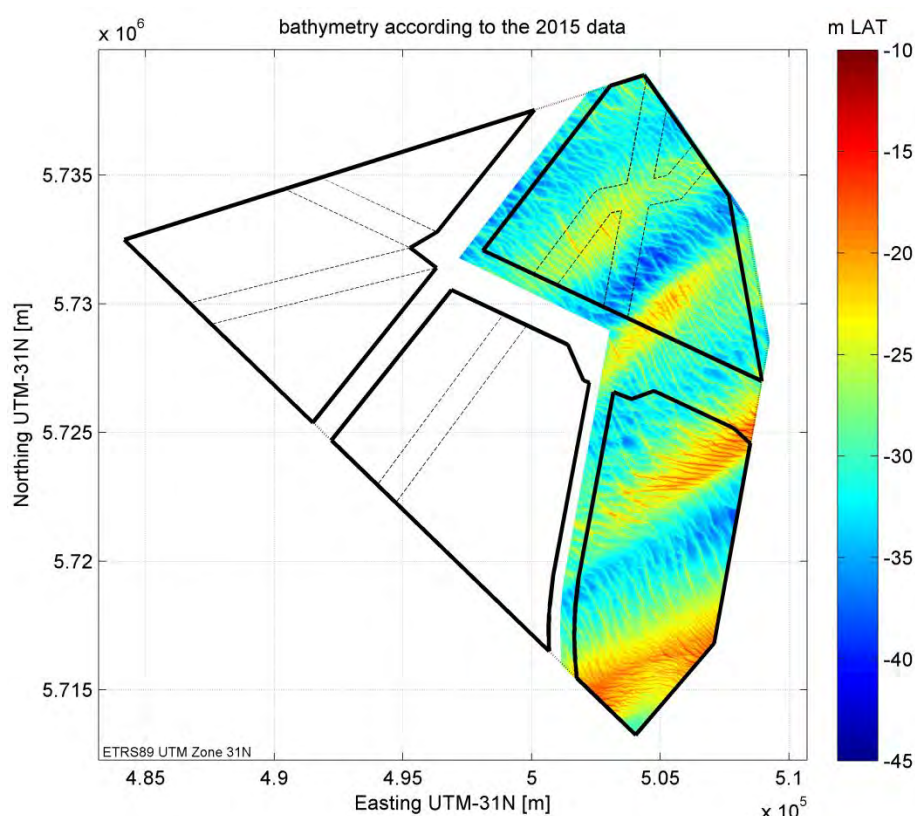


Figure 2.2 Bathymetry of WFS-I and WFS-II as recorded by Deep (2015a, 2015b). Bed levels are given in meters relative to Lowest Astronomical Tide (LAT). Note that no overlapping data at the outer edges of the BWfZ is recorded.

2.4 Geodetic parameters

Similar to the previous study by Deltares (2014) and the survey reports by Deep (2015a, 2015b) all geographical coordinates are based on the ETRS1989 horizontal datum, which is based on the GRS80 ellipsoid, and the UTM 31N projection. Vertical levels are relative to Lowest Astronomical Tide (LAT); see Table 2.2 for the parameters.

Parameter	Value
Horizontal datum	ETRS89 (EUREF89)
Spheroid	GRS 1980
Spatial Reference System Identifier EPSG	4258
Semi-major axis (a)	6378137.00m
Semi-minor axis (b)	6356752.314m

Inverse flattening (1/f)	1298.257222101000
Flattening (f)	0.003352810681182
First eccentricity	0.081819191042816
First eccentricity squared (e2)	0.006694380022901
Second eccentricity (e')	0.082094438151917
Projection	UTM zone 31 North
Latitude of grid origin	0° 00' 00.000"
Longitude of grid origin	3° 00' 00.000"
Grid Easting at grid origin	500000
Grid Northing at grid origin	0.00
Scale factor at longitude of origin	0.9996
Vertical datum	LAT GEONZ97 (Noordzee

Table 2.2 Geodetic parameters used in this study (similar to Deltares (2014) and Deep (2015a, 2015b)).

2.5 Generic characterization of morphodynamic seabed features

Large parts of the sandy seabed of shallow seas, such as the North Sea, are covered with rhythmic bed patterns. These bed patterns are the result of the complex interaction between hydrodynamics, sediment transport and morphology. Typical parameters as wavelength, wave height, mobility and, following from the combined effect of these first three, the potential threat to foundations and electricity cables, are presented in Figure 2.3.

Ripples are the smallest and fastest migrating seabed features, but because of their limited size they can be disregarded in the analysis. Ripples are, however, relevant for the bed roughness and sediment transport in the area. Megaripples are larger with a height of a few decimetres up to 1m. Because of their relatively short wavelength and high migration speed, a turbine foundation will experience many megaripples passing during the lifetime of a wind farm. So, if the sand waves and sand banks would be completely stable (or if sand waves would be non-existent), seabed variations are at least in the order of the height of the megaripples.

Sand waves and sand banks both have dimensions which are significant for foundation design. Where the sand banks often can be considered to be stationary for the lifetime of a wind farm, the sand waves typically migrate fast enough to cause meters of seabed variation, depending on the location on the sand wave. Therefore, the focus of this study will be mainly on sand waves.

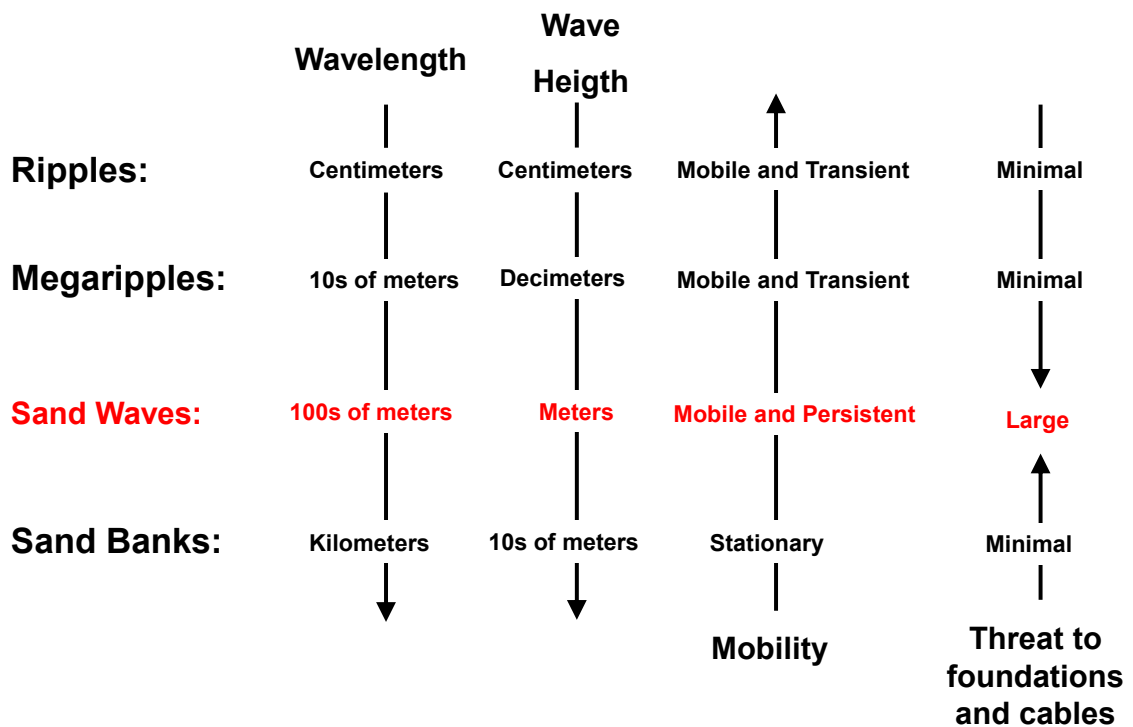


Figure 2.3 Morphodynamic seabed features in BWFZ and some typical characteristics.

2.6 Background information on sand waves and their physical processes

Typical sand wave characteristics

As explained in the previous section, most threatening large scale bed patterns to offshore structures are tidal sand waves, which may grow up to 25% of the water depth (McCave, 1971), have wavelengths (distance between two successive crests) in the order of hundreds of meters (Van Dijk and Kleinhans, 2005), migrate at a speed up to tens of metres per year (Dorst et al., 2009) and can regenerate after dredging in several years (Knaapen and Hulscher, 2002). In the Southern North Sea, sand waves are observed in water depths in the order of 20-40m, flow velocity amplitudes of around 0.65m/s and median grain sizes of 0.35mm (Borsje et al., 2009).

Modelling of sand wave processes: growth, decay and migration

Hulscher (1996) showed that sand wave formation can be explained as an inherent instability of the sandy seabed subject to tidal motion. The interaction of the oscillatory tidal current with a bottom perturbation gives rise to a tide-averaged residual circulation directed from the trough towards the crest of the sand wave (see Figure 2.4). This residual circulation induces a net sediment flux towards the crest of sand waves, which lead to sand wave growth if it overcomes the opposite effect of gravity. The migration of sand waves is caused by an asymmetry in the residual circulation cells, due to tidal asymmetry and residual currents (Németh et al., 2002 and Besio et al., 2004).

The model by Hulscher (1996) describes the hydrodynamics by using the three-dimensional shallow water equations. The turbulent stresses are accounted for by combining a constant eddy viscosity with a partial slip condition at the bed and sediment transport is only modelled as bed load transport. Despite the strongly schematized representation of the physical processes, the occurrence of sand waves in the Southern North Sea was predicted

reasonably well (Hulscher and van den Brink, 2001). In the model a constant eddy viscosity in combination with a partial slip condition at the bed is adopted. Besio et al. (2006) extended the model proposed by Hulscher (1996) by introducing a depth-dependent eddy viscosity in combination with a no-slip condition at the bed. Moreover, both bed load and suspended load are included in the model, showing an opposite effect on sand wave formation (growth and decay respectively). Comparison of the model outcome with field data showed that the model was able to reproduce the sand wave length at different locations on the Belgium Continental Shelf fairly well (Cherlet et al., 2007).

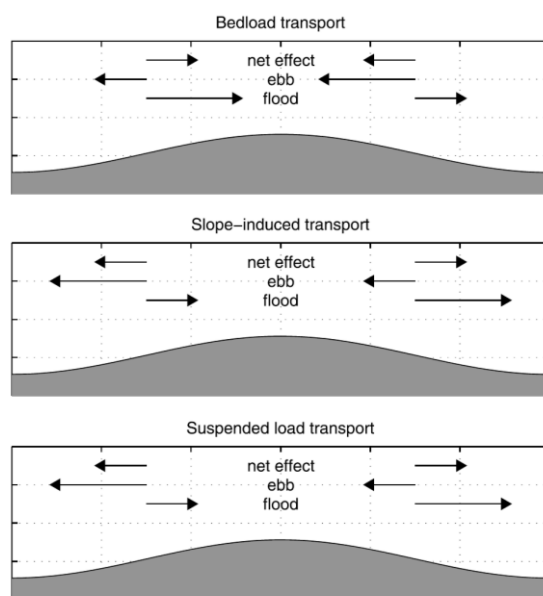


Figure 2.4 Schematic overview of the three dominant processes in sand wave formation: bed load transport (net flux towards the crest: causing sand wave growth), slope-induced transport (causing sand wave decay), and suspended load transport (causing sand wave decay). Distinction is made between the fluxes during the flood and the ebb phase. Fluxes and sand wave dimensions are not to scale (Borsje et al., 2014).

Sand waves may be superimposed by megaripples, which have wavelengths of tens of meters and heights up to 1m. These megaripples are flow-transverse bed patterns and migrate with a rate of about 0.5m/day (Ashley, 1990).

Bathymetric patterns of bedforms in the North Sea generally remain the same over decades. When two bathymetric maps, surveyed (more than) 10 years apart, are plotted side by side, the bed patterns are very similar. For example, the 1999-2001 and 2010 data of the Borssele site show similar large-scaled patterns of sand banks, where also the sand wave patterns are similar. That bed patterns remain the same over decades also follows from examples of bathymetric cross sections in the southern North Sea over offshore sand banks with superimposed sand waves (e.g. Figure 3.24 in Van Dijk et al., 2011). Notwithstanding the similarity of the general pattern, previous studies - quantifying geometric and dynamic parameters of individual sand waves in time - report differences in sand wave lengths, heights, shape and migration rates in subsequent periods (e.g. Sterlini et al., 2009; Van Dijk et al., 2011).

Sand wave lengths may change a few to tens of meters between surveys in time, but compared to their wavelengths of hundreds of meters, this change may be insignificant. The

variations in lengths of adjacent sand waves in one area are larger than the changes in lengths of individual sand waves in time.

Van Santen et al. (2011) suggested that the spatial variation in sand wave lengths may be related to current velocity, but seems unaffected by water depth and elongation of the tidal ellipse. Borsje et al. (2014) found critical conditions for sand wave formation, which are related to the dominant transport mode locally. As soon as suspended load is the dominant transport mode, sand wave fields are absent. The lower limit of sand wave occurrence is found at a Rouse number of 1.9 (Rouse number is defined as the ratio between sediment settling velocity and shear velocity), which roughly corresponds to a situation in which the grain size is smaller than 0.225mm or the flow velocity amplitude becomes larger than 0.775m/s.

Sand wave heights may change following sand wave growth or decay, due to the seasonal variation in environmental parameters (Buijsman and Ridderinkhof, 2008a; 2008b) or storms (e.g. Houthuys et al., 1994; Sterlini et al., 2009; Sterlini et al., 2012). Differences in height may be short term (yearly or event-related) and long term (decades) and may be in the orders of decimeters to meters.

For sand waves in the tidal inlet Marsdiep (water depths around 24m below MSL, average wavelength 190m, average height 3m), determined from a high temporal resolution time series between 1998 and 2005, Buijsman and Ridderinkhof (2008b) found a seasonal variation in sand wave height, where sand waves were 0.5m lower in spring compared to autumn.

Variations in growth and decay were also reported at offshore locations, for example offshore Rotterdam at a water depth of 30m below LAT, some sand waves decrease in height in the period 1999-2002 and then increase in height in the period 2002 – 2007 (e.g. site 1 in Van Dijk et al., 2011). Further offshore, at the North Hinder Traffic Separation Scheme and at water depths of approximately 33m below LAT, sand waves with an average wavelength of 270 m and average wave height of 4.8m were found to grow steadily in height (Van Dijk et al., 2011). Here, the crest heights of sand waves increased with roughly 2m in the period between the early 1990s and 2006.

The change in the asymmetry of sand waves was studied for sand waves offshore Rotterdam, where a very subtle increase in the averaged asymmetry index in time was found (see Figure 2.5). With similar lengths and heights, an increase in the asymmetry index ($AI = \text{length of stoss side} / \text{length of lee side}$) reveals that the stoss sides become more gentle and the lee sides steeper.

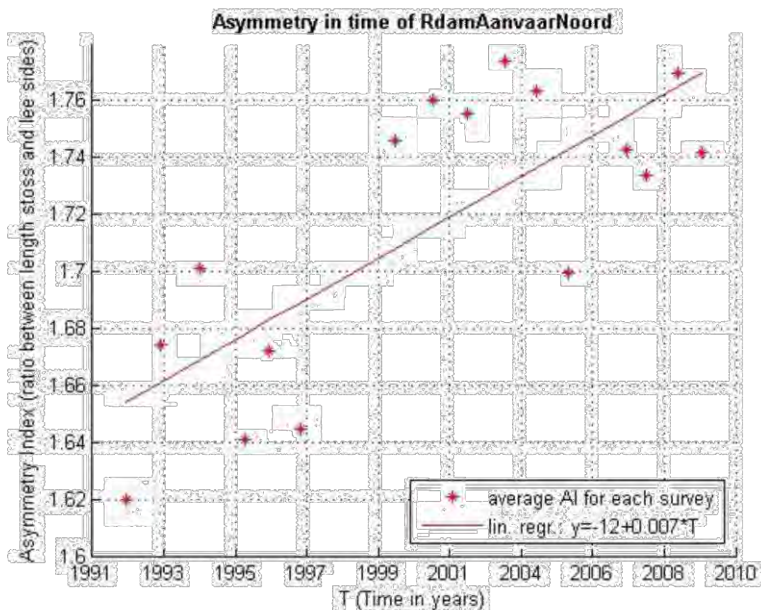


Figure 2.5 Averaged asymmetry indices of sand waves in time for a profile offshore Rotterdam, showing a very subtle increase in a period of less than 10 years. The averaged asymmetry index, AI = length of stoss side/length of lee side, increases from 1.65 to 1.75.

An increase in asymmetry was reported at other locations, such as on the UK shelf (Sterlini et al., 2012). However, in a sand wave field 50 km offshore Egmond, the asymmetry was found to decrease (Van Dijk and Kleinhans, 2005). Whether such a change in shape also occurs at the Borssele site, needs to be investigated. The asymmetry of sand waves may be related to the migration rate of sand waves (Knaapen, 2005).

Apart from the spatial variation in dynamic behaviour of sand waves (e.g. Van Dijk and Kleinhans, 2005; Van Dijk and Egberts, 2008; Dorst et al., 2011), the migration direction and migration rates of sand waves may vary in time at one location (e.g. Van Dijk et al., 2011). The migration direction of sand waves is generally in the direction of the residual current, but may reverse due to higher tidal constituents (Besio et al., 2004) or – in coastal settings – due to advection of sediment and estuarine circulation (Buijsman and Ridderinkhof, 2008b).

Migration rates depend on the residual current velocity, but may also be controlled by wave action, both by the stirring of sediment and thereby adding to the sediment transport, increasing migration rates (Van Dijk and Kleinhans, 2005), and by the directions of the waves with respect to the residual tidal current, thereby decreasing migration rates when wave and current directions are opposed (Sterlini et al., 2012).

In general, the morphology of sand waves (lengths, heights, steepness and asymmetry), as well as changes in dynamics (growth, migration) can change in time, e.g. due to seasonal influences and occurrence of storm events (Deltares, unpublished data). The measured bathymetry may therefore depend on when surveys were carried out.

The effects of storms on sand wave characteristics still remains to be investigated. Few studies report that storms will lower the sand wave heights due to the action of surface waves. In a study on the Middelkerke Bank on the Belgian Continental Shelf, with observations before and after a storm at water depths of 10 to 15m, Houthuys et al. (1994)

found that the crests of 1-3m high sand waves on the top of the bank decreased in height by 0.3 - 1.2m as an effect of storms with deposition in the adjacent troughs, thereby smoothing the morphological profile and causing sand wave migration towards the top of the bank. Also, megaripples with heights of 0.2-0.5m on the north-west flank of the bank disappeared after the storm. However, in some parts, both deep and shallow, the smoothing was not significant. On the other hand, storms may also create bedforms, such as hummocks, which are 3-dimensional bedforms with wavelengths in the order of meters (Passchier and Kleinhans, 2005; Peters and Loss, 2012).

Under high surface waves, sediment is stirred up and is transported by the tidal current. Van Dijk and Kleinhans (2005) show in sensitivity plots that the orbital motion at the bed below surface waves of 3m high is sufficient to cause sediment transport at the bed at 25m water depth for sediment grain sizes of up to 300 micrometer. Records of significant wave height in the shallow Southern Bight of the North Sea reveal that surface waves of 3m occur several times per year, mostly during winter seasons. During periods of fair-weather conditions, the height of sand waves may then again increase (Terwindt, 1971; Buijsman and Ridderinkhof, 2008a). Therefore, both the magnitude and frequency of storms play a role in the reduction of sand wave heights.

The increased sediment transport due to high surface waves also influences the migration rate of sand waves (Van Dijk and Kleinhans, 2005; Sterlini et al., 2012). Opposing directions of wave propagation and tidal currents may decrease the migration rate. An additional factor affecting the migration rate of sand waves is the wind- and surge-driven current, which increases the sediment transport during storms and causes sedimentation in the waning stage of the storm (Papilli et al., 2014).

Current research projects specifically investigate the impact of storms on sand wave geometry and dynamics, both in empirical and modelling approaches (e.g. NWO research project SMARTSEA and SANDBOX).

In summary, the large-scaled bathymetric patterns remain more or less similar over decades, but (temporary) changes may occur. The changes in length, height, steepness and asymmetry of individual sand waves are variable in time, and may be opposite in subsequent periods between surveys. Net changes of a period of decades may therefore be more steady, because the short-term variations are averaged out. As seasonal changes may occur (mainly related to occurrence of severe storms), they should be sufficiently covered in this study in the adopted methodology and uncertainty ranges.

2.7 Characterization of Borssele Wind Farm Zone

The Borssele Wind Farm Zone is located in the southern part of the Dutch North Sea, near the Dutch-Belgian border (see Figure 2.6). The area is divided into 4 development sites (site I, site II, site III and site IV, named clockwise starting with the north-eastern site), which are subdivided into a total of 10 sub-sites due to the presence of offshore line infrastructure (see Figure 2.7 and Figure 2.8).

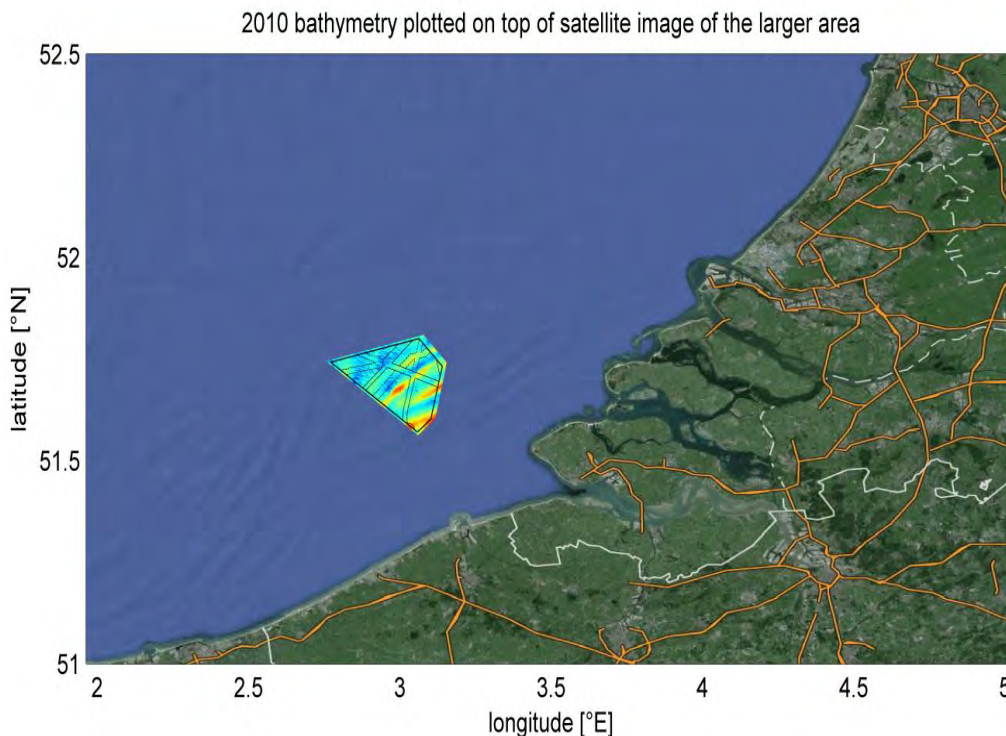


Figure 2.6 Location of the Borssele Wind Farm Zone in the southern part of the Dutch North Sea.

Bed levels in the area vary between -12.6m and -42.2m relative to Lowest Astronomical Tide (LAT). The BWFZ has a diverse morphology with shore-perpendicular sand waves on top of shore-parallel sandbanks of over 10m in height (see Figure 2.8). The presence of sand waves is consistent throughout the area, with the exception of a small patch in the southernmost corner of site II. General maps characterizing morphodynamic features at the seabed, such as Figure 2.9, show that in the BWFZ sand waves occur with heights between 2-4m around the Rabsbank, with heights between 4-6m around the Schaar Sandbank and with heights larger than 6m in the more offshore located areas.

Close to the BWFZ, in the Belgian part of the North Sea, wind farm development has started some years ago (e.g. Thornton Bank and Belwind are operational with other parks still under development). Studies for these developments indicate complex morphodynamic activity in the area. A study by TNO (this particular department has now merged into Deltares), described in Wiertsema & Partners (2008), on the stability of the Bligh Bank (located just across the border, southwest of site IV), found opposing bed form migration directions, with sand wave lengths in the order of 200m, sand wave heights in the order of 4m and sand wave migration speeds of up to 2.5m/yr. A study by Deltares for the Belwind development found similar morphodynamic behaviour and sand wave dimensions (Deltares, 2008), corroborating the findings for the Borssele Wind Farm Zone in this report.

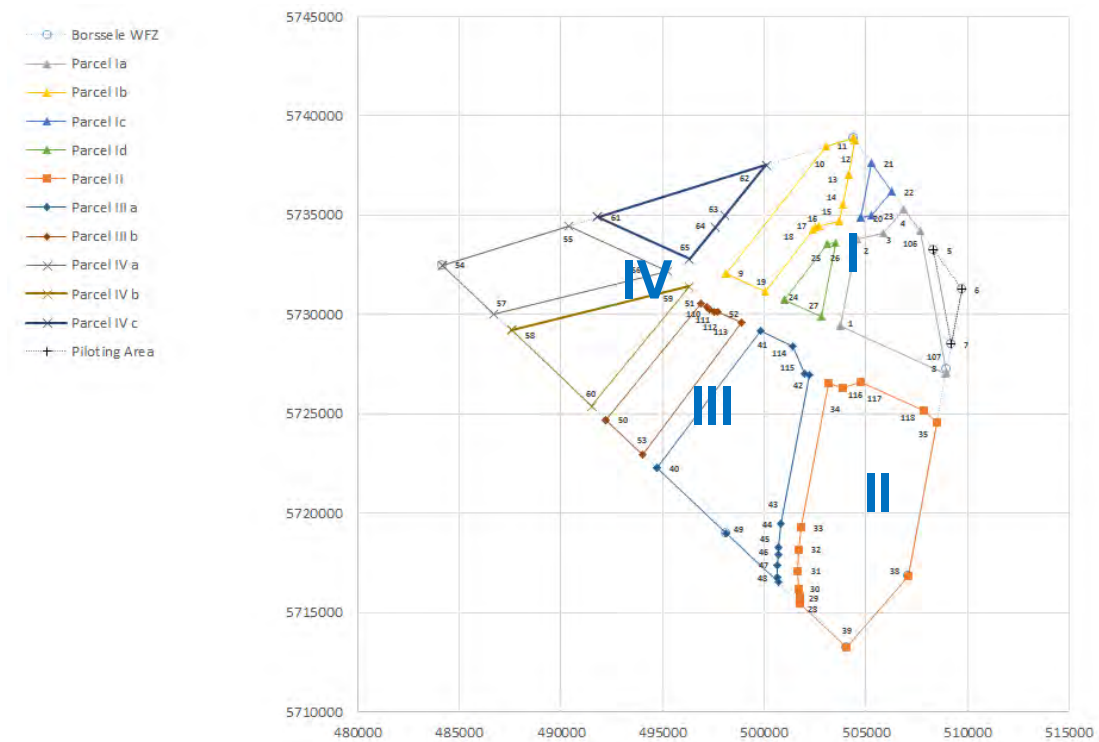


Figure 2.7 Overview of (sub-)site division in the Borssele Wind Farm Zone and safety zones related to telecommunication and electricity cables [data delivered by RVO; version 4 May 2015].

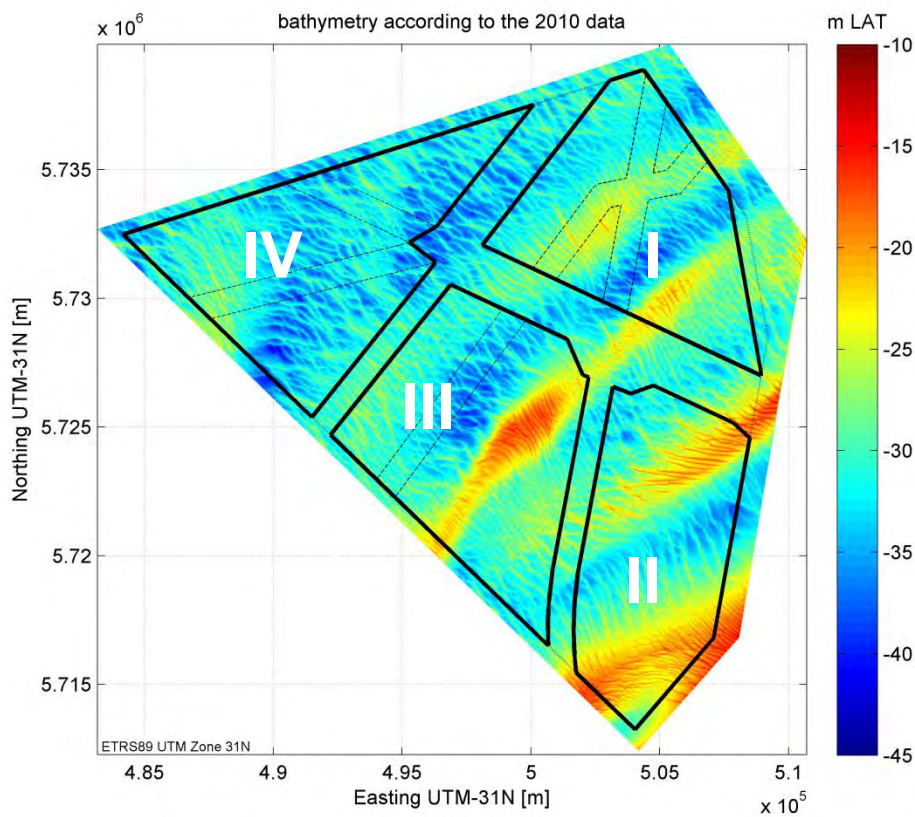


Figure 2.8 Bathymetry according to the 2010 survey. Bed levels are given in m LAT.

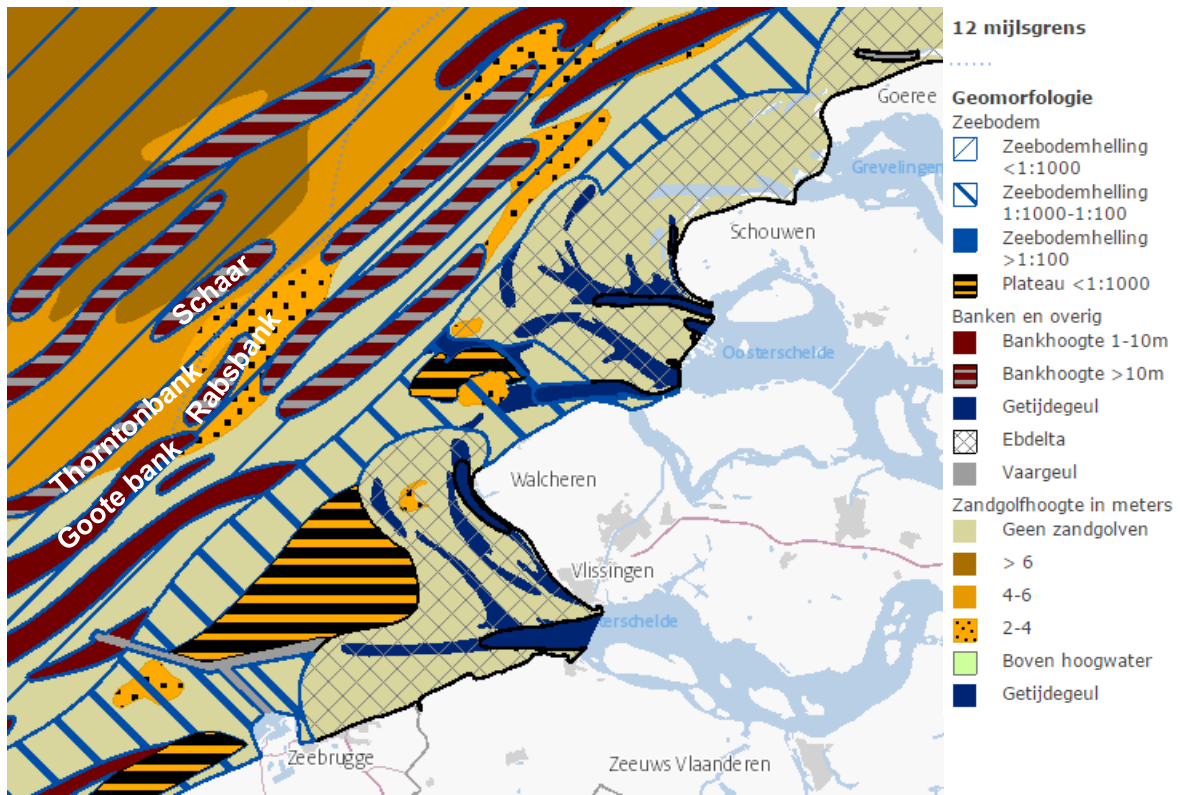


Figure 2.9 Map illustrating seabed morphology in the Borssele Wind Farm Zone [extracted from Noordzeeatlas.nl, underlying data was derived from Van Alphen&Damoiseaux, 1989; names of sandbanks were added in white].

3 Data analysis and pre-processing for sand wave analysis

3.1 Introduction to methodology

In BWFZ several morphodynamic seabed features can be found, i.e. seabed ripples, megaripples, sand waves and sand banks. Typical parameters as wavelength, wave height, mobility and, following from the combined effect of these three, the potential threat to foundations and electricity cables, were presented in Figure 2.3 and Section 2.5.

Since the sand waves are both large and sufficiently mobile, the sand waves will be analysed thoroughly in this study. The subsequent steps to prepare the bathymetrical data for the sand wave analysis are presented in this chapter. The sand wave analysis itself is described in the next chapter. The final goal is to derive two Design Seabed Levels, which are required as input parameter for many (structural) design aspects:

- 1 Reference SeaBed Level (RSBL), which is the expected lowest possible seabed level in the BWFZ during the period 2015-2046;
- 2 Maximum SeaBed Level (MSBL), which is the expected highest possible seabed level in the BWFZ during the period 2015-2046.

If both levels are compared with the present bathymetry (2015), the expected maximum seabed lowering (present bathymetry – RSBL) and the expected maximum seabed rising (MSBL - present bathymetry) can be derived. In order to predict these levels for the BWFZ, the following techniques were used:

1. Large-scale bathymetric filtering to distinguish between the “static” and “mobile” seabed features (Section 3.2);
2. Filtering and analysis of megaripples (to be part of the uncertainty band) (Section 3.3);
3. Extraction of the sand wave field (sand banks and megaripples excluded) for sand wave analysis (Section 3.4);
4. Automated detection of sand wave migration directions (Section 4.2);
5. Fourier analysis on individual sand waves to determine sand wave migration rates (Section 4.3);
6. Estimating uncertainty range based on measurement errors, processing inaccuracies and smaller scale seabed features such as megaripples (Section 5.2);
7. Migration of sand wave fields with calculated migration rates and directions (Section 5.3);
8. Combining migrated sand wave fields with “static” bathymetry and uncertainty range to compute RSBL and MSBL (see Sections 5.4 and 5.5);
9. Comparing the isopach of the base of the Holocene Formation with the RSBL to avoid overly conservative downward bed level changes (Section 5.6);
10. Translate RSBL and MSBL into zones with various recommendation levels for offshore foundations and cables (Section 5.7);

Steps 1 to 3 are explained and illustrated in this chapter. The methodology and results of steps 4 and 5 are discussed in Chapter 4. Steps 6 to 10 are described in Chapter 5.

In the remainder of this document we will use the definitions of the various spatial bathymetrical data fields as explained in Table 3.1.

Short name	Description	Sand banks	Sand waves	Mega-ripples
2015 bathymetry	Full measured bathymetry by Deep in 2015			
Static bathymetry	Long-term mean bathymetry (for the considered period / lifetime of wind farms)			
Quasi-static bathymetry	Bathymetry with megaripples filtered out			
Mobile bathymetry	Mobile bathymetry (sand wave directions + Fourier analysis +)			
Sand Wave field	Sand wave field (to migrate future bathymetries, RSBL, MSBL)			
Megaripple field	Megaripple field (uncertainty band)			

Table 3.1 Definitions of various bathymetrical data fields used in this study.

Remark on cross-correlation technique and $\delta z/\delta t$ -analysis mentioned in proposal

Originally it was assumed that a cross-correlation technique could be applied to assess the migration direction of bed forms in the Borssele area. However, due to the complex bathymetry and opposing migration directions, a somewhat different technique produced slightly better results. This different technique is discussed in more detail in Section 4.2.

A $\delta z/\delta t$ -analysis technique was also considered. This method is based on computing annual seabed variations over the entire grid and is also very useful to determine where migrating bed forms are present, as is illustrated in Figure 3.1. This figure shows the bed level differences over a period of 9-11 years, dependent on the year of the first survey that was used in this analysis. It can clearly be observed from the difference patterns that bed forms (i.e. sand waves) are migrating over the seabed. The length, height and migration directions of the bed forms show significant variation over the BWFZ-area. Note that due to some artificial "stripes" in the survey data (e.g. due to roll misalignment) and small differences in vertical level, this analysis is less suitable to obtain quantitative predictions for bed level variations at future WTG-locations and along cable trajectories. Besides, when migrating bed forms are present, the $\delta z/\delta t$ -analysis technique can be overly conservative when predicting over long time intervals due to the rhythmic seabed variation over time (periods of alternating rising and dropping seabed levels). Because sand waves are present over the almost complete BWFZ-area, this method is not used in this analysis.

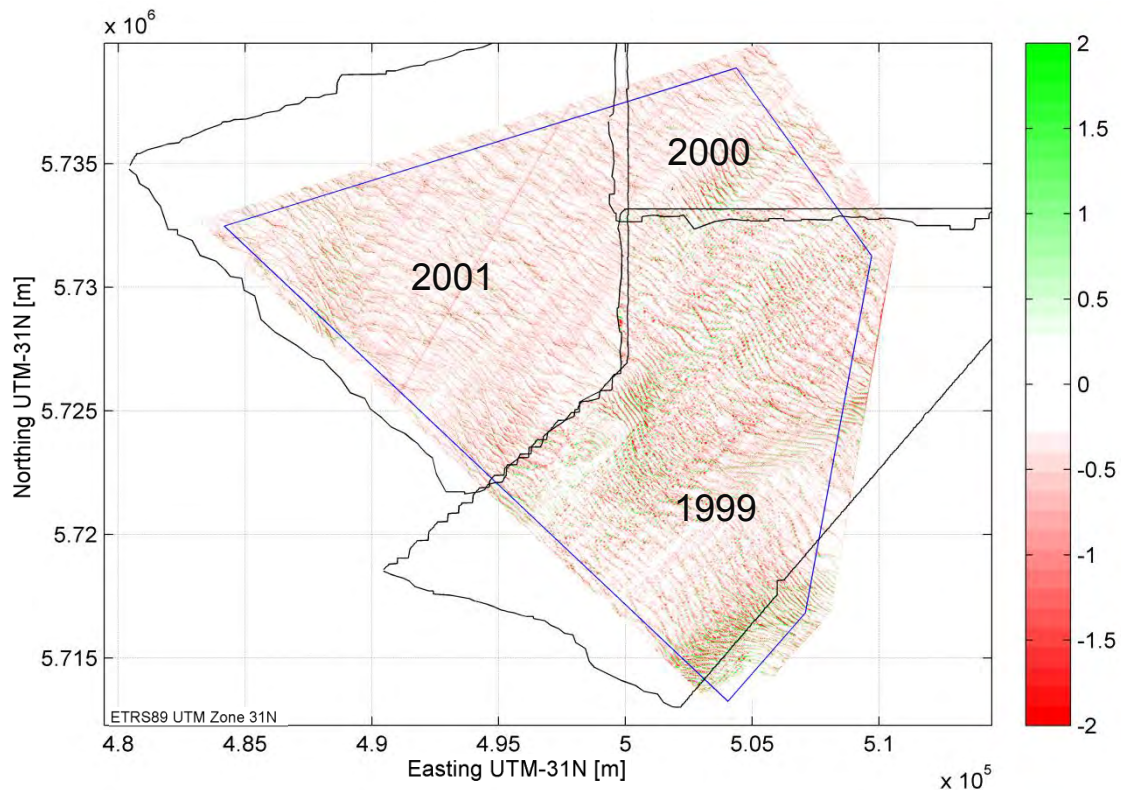


Figure 3.1 Example of $\delta z/\delta t$ -analysis: difference plot over 9-11 year period (depending on the surveyed area). The polygons indicate the different years of the first survey that was used in the analysis.

3.2 Large-scale bathymetric filtering

The first step is to isolate the higher frequency migrating sand waves from the sand banks. For this purpose a coarse spatial filtering of the bathymetry was applied on all available surveys. The filter size was chosen such that the mobile bed forms (i.e. sand waves and megaripples) could be removed by filtering, while the sand banks should still remain their shape and not noticeably be smoothed by the filtering process. Because the sand waves have an average crest orientation around the SE-NW-axis and the sand banks have an average orientation more or less perpendicular to the sand waves, it was decided to use an ellipsoid with the long axis under an angle of 45°N. The filter size along the long axis was chosen at 1000m, while the filter size along the short axis was only 50m. In this way, averaging over the sand waves did not cause too much smoothing of the sand banks, while a filter size of 1000m is longer than the longest observed sand wave lengths in the BWFZ, ensuring that all sand waves are filtered out.

The results for all three bathymetries are shown in Figure 3.2. The left column of plots depicts the Measured Bathymetries in 2000, 2010 and 2015, while the middle column shows the filtered result. These bathymetries can be considered as long-term mean bathymetries around which the sand wave elevations fluctuate (analogous to a Mean Sea Level around which the water wave elevations fluctuate). These bathymetries only show the tidal channels and sand banks, while the sand waves are filtered out. In the remainder of this report these bathymetries are referred to as Static Bathymetry, because this long-term mean bathymetry is considered to remain constant throughout the considered period of 2015-2046. Please be aware that the term “static” does not mean that the seabed sediment will not become mobile below this level.

Note that the middle lower plot, depicting the Static Bathymetry in 2015, shows some white edges at the outer edges of the BWFZ. This is caused by the fact that bathymetry data was only recorded right until the edge, without any overlap at the BWFZ-boundary, while the filtering process requires a certain overlap related to the filter size. This problem was solved by substituting 2010-bathymetrical data at the edges, which has negligible influence on the determination of the Static Bathymetry.

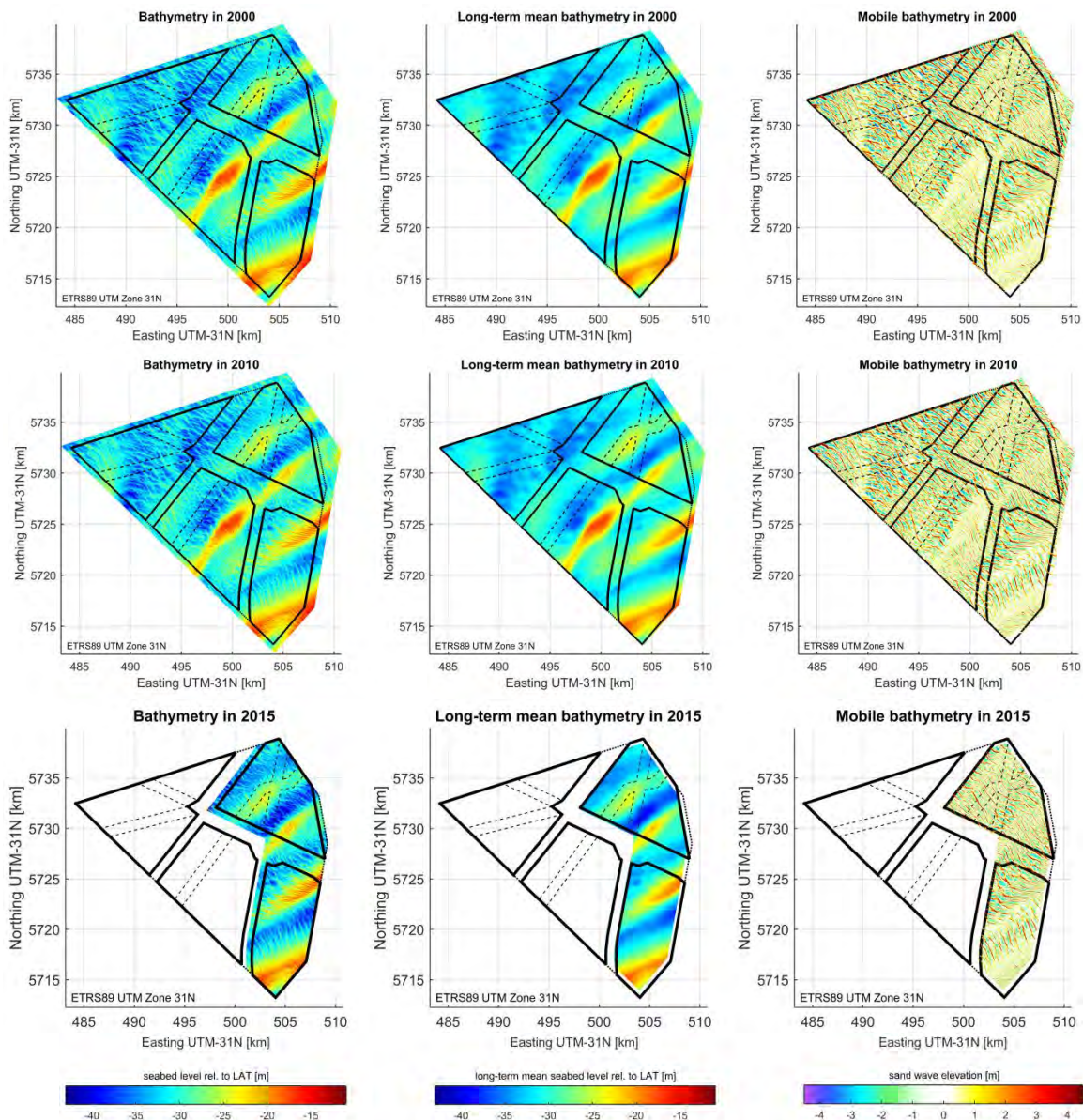


Figure 3.2 Filtering of bathymetries of 2000 (top row), 2010 (middle row) and 2015 (bottom row) to derive from the Measured Bathymetries (left column) the Static Bathymetries (middle column) and the Mobile Bathymetries (right column).

Finally these Static Bathymetries were subtracted from the Measured Bathymetries. Then the Mobile Bathymetries remain, which consist of the Sand Wave Field and the Megaripple Field. It can be observed that the resulting data fields have a zero mean with amplitudes fluctuating

around zero. Note that the observed wave patterns represent the sand wave fields; in order to see the megaripples, you need to zoom in significantly. The Mobile Bathymetries have been used as input for the sand wave analysis in Chapter 4.

To check whether the assumption of a Static and Mobile Bathymetry is valid the three Static Bathymetries have been subtracted from each other in Figure 3.3. It can be observed that the visible patterns are only related to the filtering process (thin ellipses under a 45° angle) and not to growing, decaying or migrating sand banks. Compare, for instance, the difference plot in Figure 3.1 where the patterns (apart from some multi-beam related striping) are clearly related to migrating sand waves. It is therefore considered realistic to assume that the sand banks and tidal channels in the BWFZ are static in typical lifetimes of offshore wind farms in the order of up to 30 years.

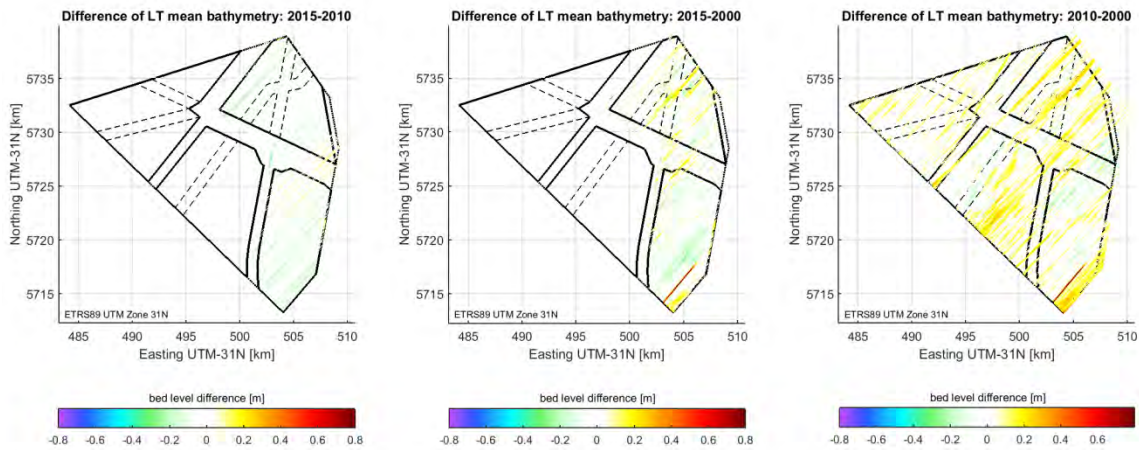


Figure 3.3 Difference plots of Static Bathymetries to check whether these bathymetries are indeed static in the period 2000-2015.

3.3 Analysis of megaripples

As explained in Section 2.5 megaripples have migration speeds that are so large that many megaripples will pass at each foundation throughout the lifetime of wind farms. Therefore, it was decided not to predict the migration of the megaripples, but to analyse the megaripple field and include some representative statistical values in the uncertainty band (see also Section 5.2).

Megaripples in the OWBZ have typical wavelengths of 8 to 15m. Since most of the analysis of the sand waves is based on 5x5m grid resolution and filtering works best for odd filter window sizes (to obtain a filter centred around the actual measurements), the bathymetry was filtered with a 15x15m window size (a normal *block averaging* filter) to obtain a sand wave field with the megaripples filtered out. For the analysis of the megaripples both wind farm sites (WFS-I and WFS-II) were analysed using a 1x1m grid in order to better capture the megaripple shapes. Note that this fine grid resolution of 1x1m is only available for the 2015-data.

In Figure 3.4 and Figure 3.5, two examples of this filtering method are presented for WFS-I and WFS-II respectively. The left images in both figures show the measured bathymetries and the middle images the filtered bathymetries. If the data is subtracted, then the megaripple field is obtained. Note that these figures are greatly zoomed in to show the megaripple with their relatively short wavelengths and small wave heights compared to the sand waves and sand banks. It can be observed that the megaripple pattern is quite irregular, dependent on the complex tide-averaged velocity patterns in this area.

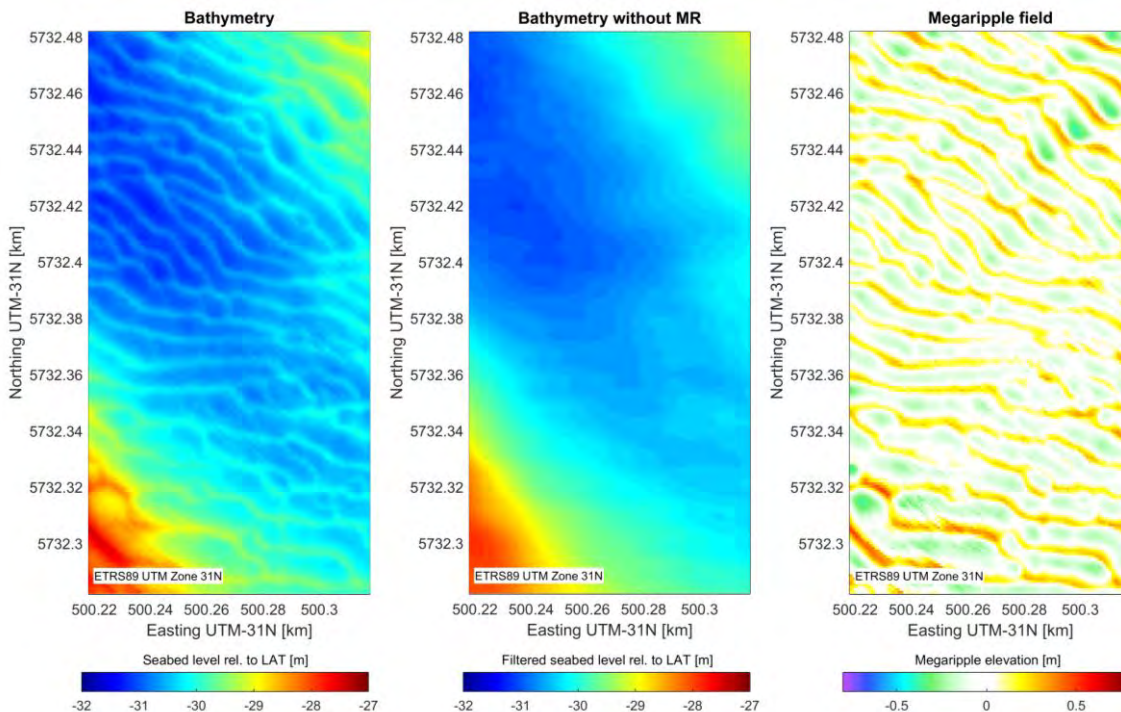


Figure 3.4 (Left) Bathymetry of WFS-I, zoomed to an area of 100 x 200m; (middle) bathymetry with megaripples filtered out; (right) megaripple field extracted from bathymetry with in orange-red showing the megaripple crests and in green-blue the megaripple troughs.

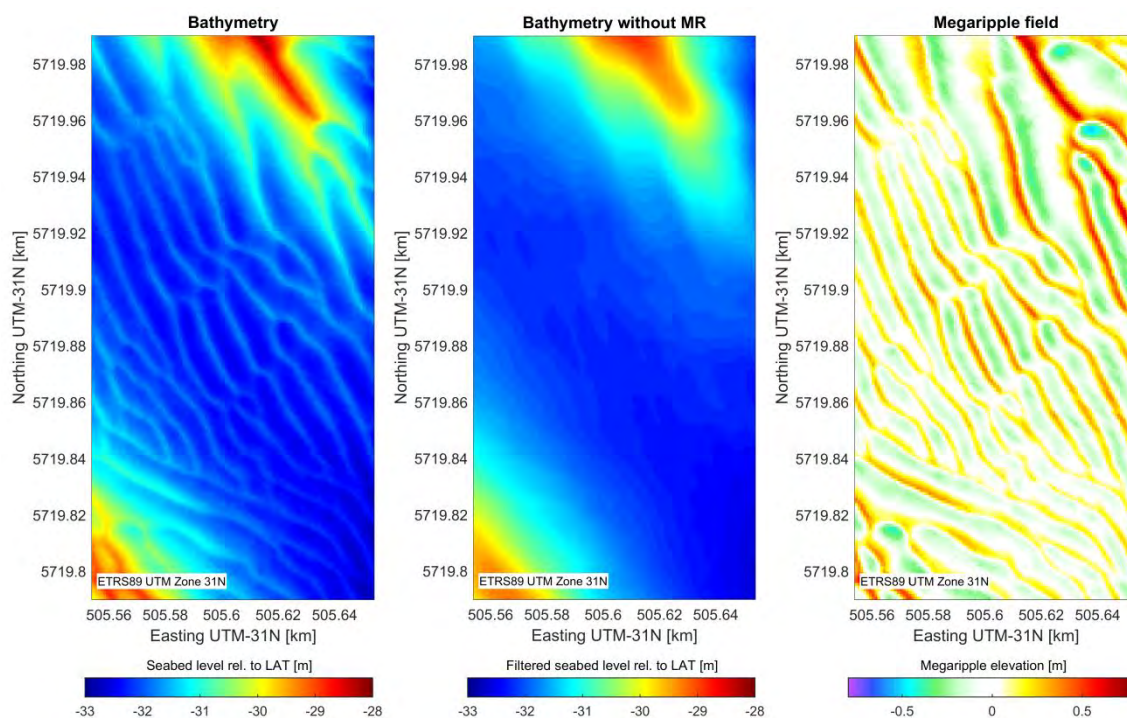


Figure 3.5 (Left) Bathymetry of WFS-II, zoomed to an area of 100 x 200m; (middle) bathymetry with megaripples filtered out; (right) megaripple field extracted from bathymetry with in orange-red showing the megaripple crests and in green-blue the megaripple troughs.

The next step is to determine the corresponding trough depths and crest heights of megaripples in BWFZ. With the same filter window size (15x15m) the minimum and maximum seabed elevations were calculated for the megaripple field. Two examples for the same areas in WFS-I and WFS-II respectively are shown in Figure 3.6 and Figure 3.7. The left images show the megaripple field again. The middle images represent the depths of the megaripple troughs when averaged over 15m blocks. Typical values range between 0.15 and 0.40m with outliers up to 0.50m.

In order to obtain the megaripple statistics for the entire area (and not just some selected areas used here for illustration), the exceedance curves for trough depth, crest height and total megaripple height are presented for both sites in Figure 3.8. The median (50%) values for the trough depth, crest height and total megaripple height are 0.22m, 0.30m and 0.54m respectively. The 95% non-exceedance values are ~0.40m for the trough depth and ~0.60m for the crest height. Note that extreme seabed levels due to passing megaripples occur only temporarily and may therefore be less relevant for fatigue analysis.

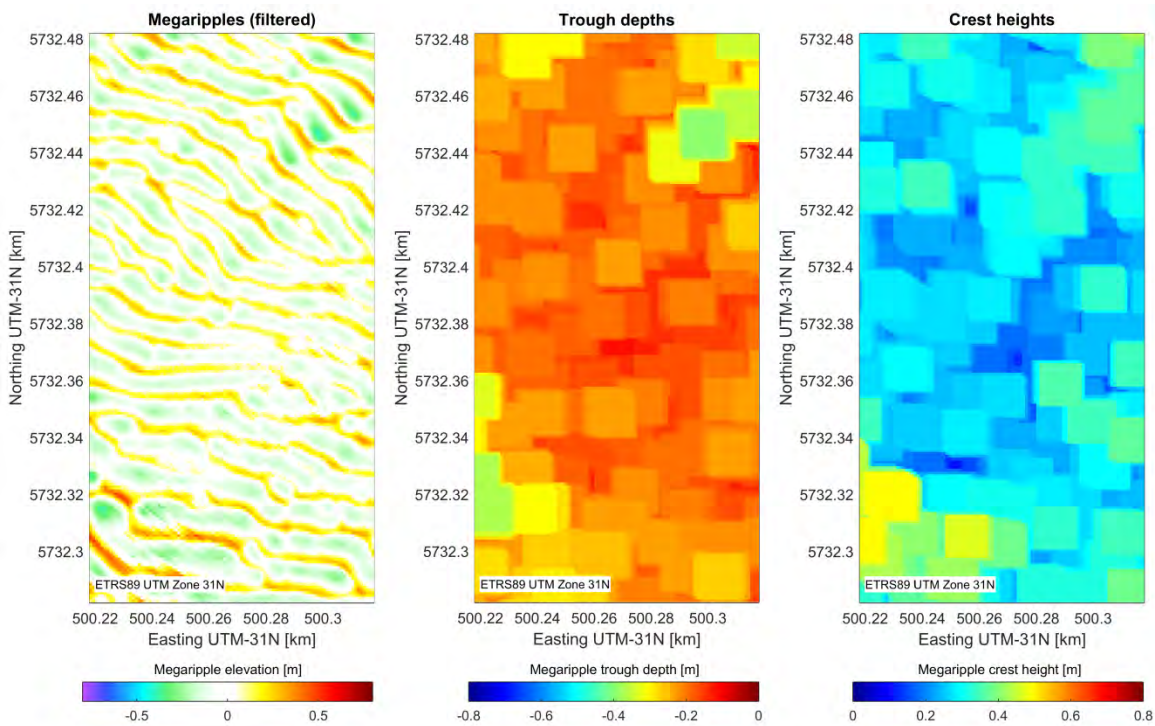


Figure 3.6 (Left) Example of megaripple field in WFS-I (right image of Figure 3.4; (middle) maximum megaripple trough depths in 15x15m areas; (right) maximum megaripple crest heights in 15x15m areas.

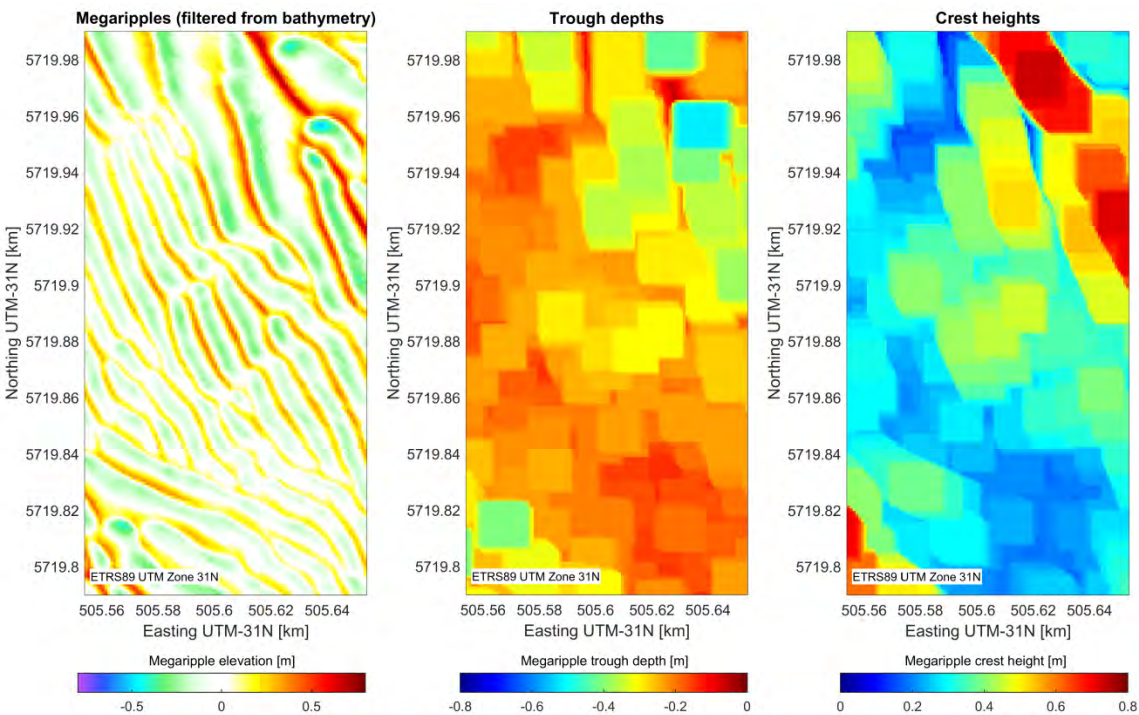


Figure 3.7 (Left) Example of megaripple field in WFS-II (right image of Figure 3.5; (middle) maximum megaripple trough depths in 15x15m areas; (right) maximum megaripple crest heights in 15x15m areas.

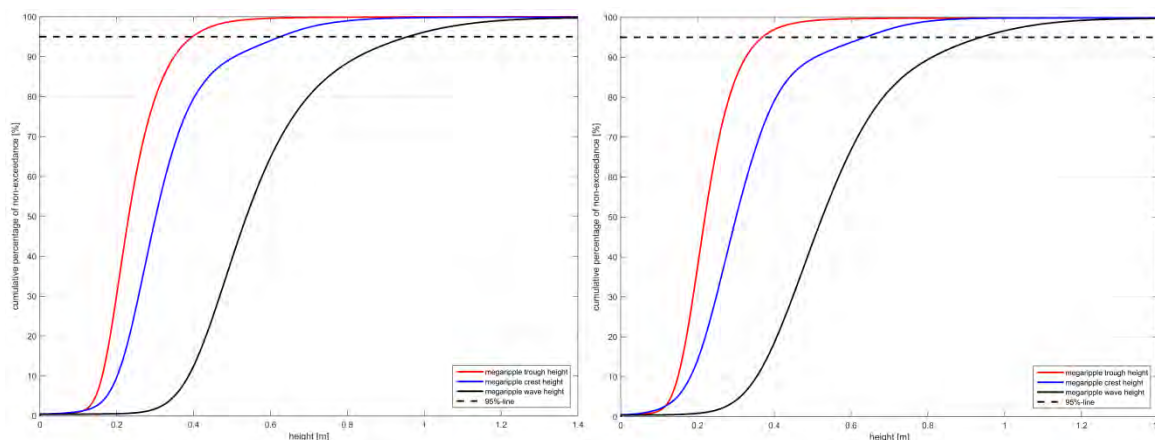


Figure 3.8 Non-exceedance curves of height of megaripple troughs, crests and complete megaripples for (left) WFS-I and (right) WFS-II.

3.4 Resulting sand wave field for sand wave analysis

For the prediction of future bathymetries the Sand Wave Field is required that does no longer contain megaripples. In the Mobile Bathymetry, obtained in Section 3.2, the megaripples were filtered out with the same filter settings as used in the megaripple analysis in Section 3.3. The remaining Sand Wave Field is plotted in Figure 3.9.

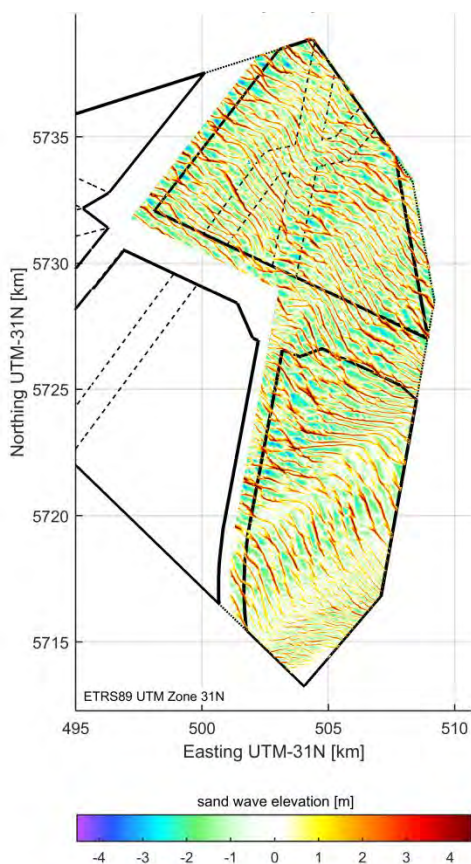


Figure 3.9 Sand Wave Field to be used for predicting future bathymetries in Chapter 5.

4 Sand wave analysis

4.1 Introduction

This chapter discusses the analysis of the sand waves in the BWFZ. Section 4.2 describes the methodology that was applied to determine the directions of sand wave migration. These directions are used to draw transects in the bathymetrical datasets. On these transects, a Fourier analysis is performed to arrive at statistics of the individual sand waves in each transect. This last step is discussed in Section 4.3.

4.2 Determination of directions of sand wave migration

In order to obtain correct sand wave transects used in the Fourier analysis (introduced in Section 4.3), the migration directions of the sand waves are required. The migration directions were determined separately for the three distinct periods between the available surveys: 2000-2010, 2000-2015 and 2010-2015.

The bed form migration direction is determined by looping over the potential migration directions of various transects using the Mobile Bathymetry. For each direction, the sand wave field derived from the older of two surveys of the considered period is migrated over several distances. For each distance case the RMS-difference between the two datasets was determined. The case with the smallest RMS-difference for the largest migration distance is considered to represent the best estimate for the migration direction. This analysis was performed for directions between 0 and 90°N with both negative and positive migration distances. This means that sand waves migrating with angles between northern and eastern direction (clockwise; 0-90°N) and with angles between southern and western direction (clockwise; 180-270°N) are covered in the analysis, representing migration along the flood and the ebb direction of the tidal current.

Due to the large complexity of the system and the observed extinction and generation of sand waves this is not a fully reliable method. However, by bulk processing a large number of points, reliable statistics can be obtained. The resulting transects and orientations are input for the Fourier analysis, which provides statistics on sand wave characteristics such as sand wave height, sand wave length and migration speed. The Fourier analysis is performed automatically on a large number of transects (665 transects displayed in the top plot of Figure 4.1) and semi-automatically on a smaller number of transects (153 transects spread further apart, displayed in the bottom plot of Figure 4.1). Therefore, the directions were determined for both the small (153) and large (665) number of transects.

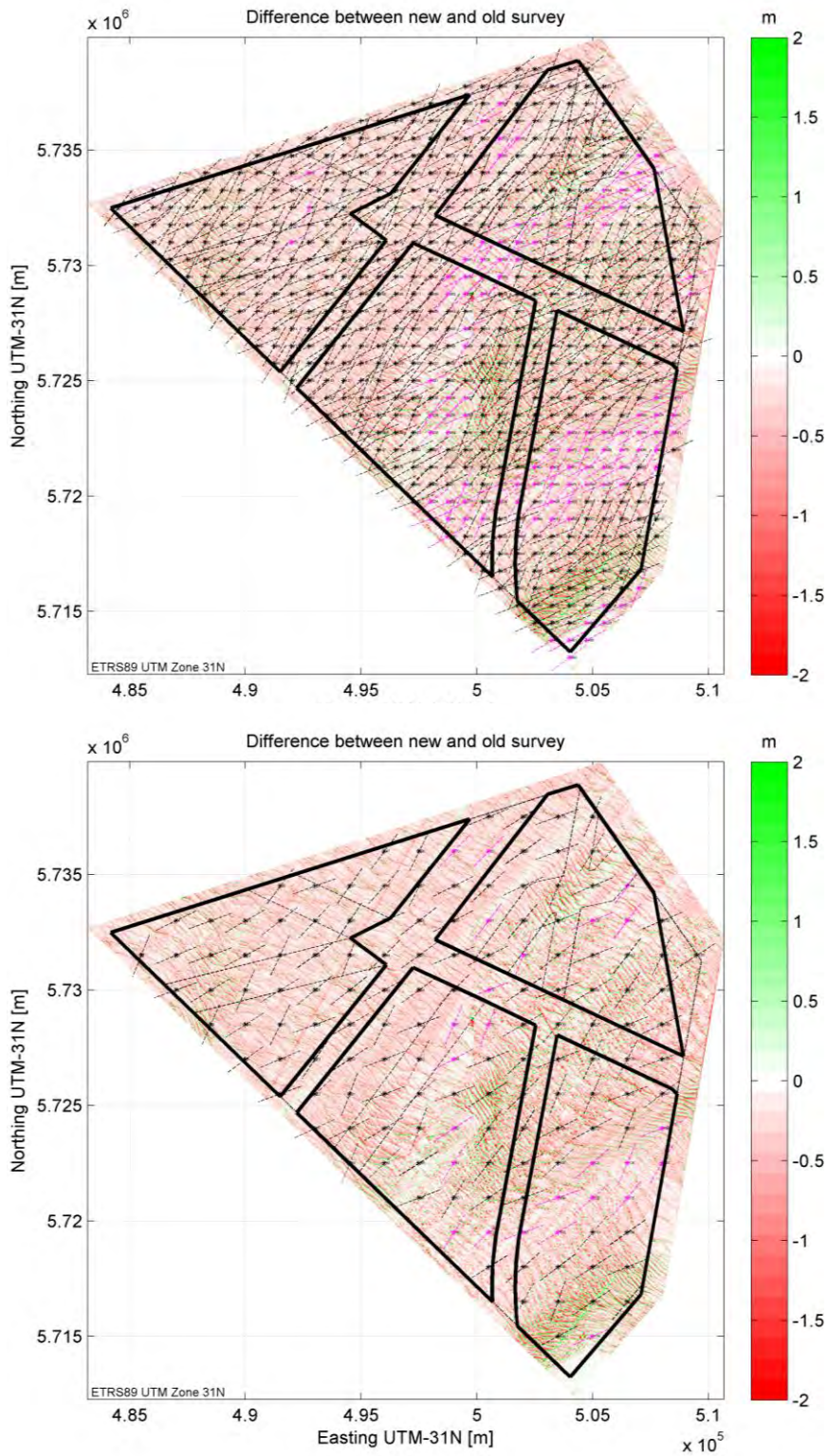


Figure 4.1 Results of the determination of the sand wave migration directions for period 2000-2010. Top plot is based on 665 transects, bottom plot on 153 transects. Black lines indicate SW-directions, purple lines NE-directions.

The results of the determination of the directions of sand wave migration for one of the three considered periods (2000-2010) are presented in Figure 4.1. The background colour of Figure 4.1 shows the difference between the 2010 and 2000 Mobile Bathymetries. The sand waves in the BWFZ are migrating to the southwest (ebb direction) as well as the northeast (flood direction), with a main axis of approximately 230° and 50° respectively (relative to north). This axis varies over the area with a variation of up to 30°. Particularly complex areas are the top of the sandbank in WFS-III and the swales in between the sandbanks in WFS-I, WFS-II and WFS-III. For illustration purposes, the rather complex migration patterns of the three considered periods have been schematized in Figure 4.2.

The migration in north-eastern direction in the swale halfway WFS-II and the swale extending all the way through WFS-III and I are most likely related to the flood tidal flow being dominant over the ebb flow, while the swale in between (passing over the south-eastern corner of WFS-I and the north-western corner of WFS-II) is most likely more dominated by the ebb current. The ebb flow is also dominant on top of the crests of the sandbanks. Similar flood- and ebb-dominated patterns were also observed in Van Lancker et al. (2013). More detailed modelling of the tidal flow patterns in this area (preferably over a full spring-neap cycle) will provide a better insight in the relation between sand wave migration and tidal flow.

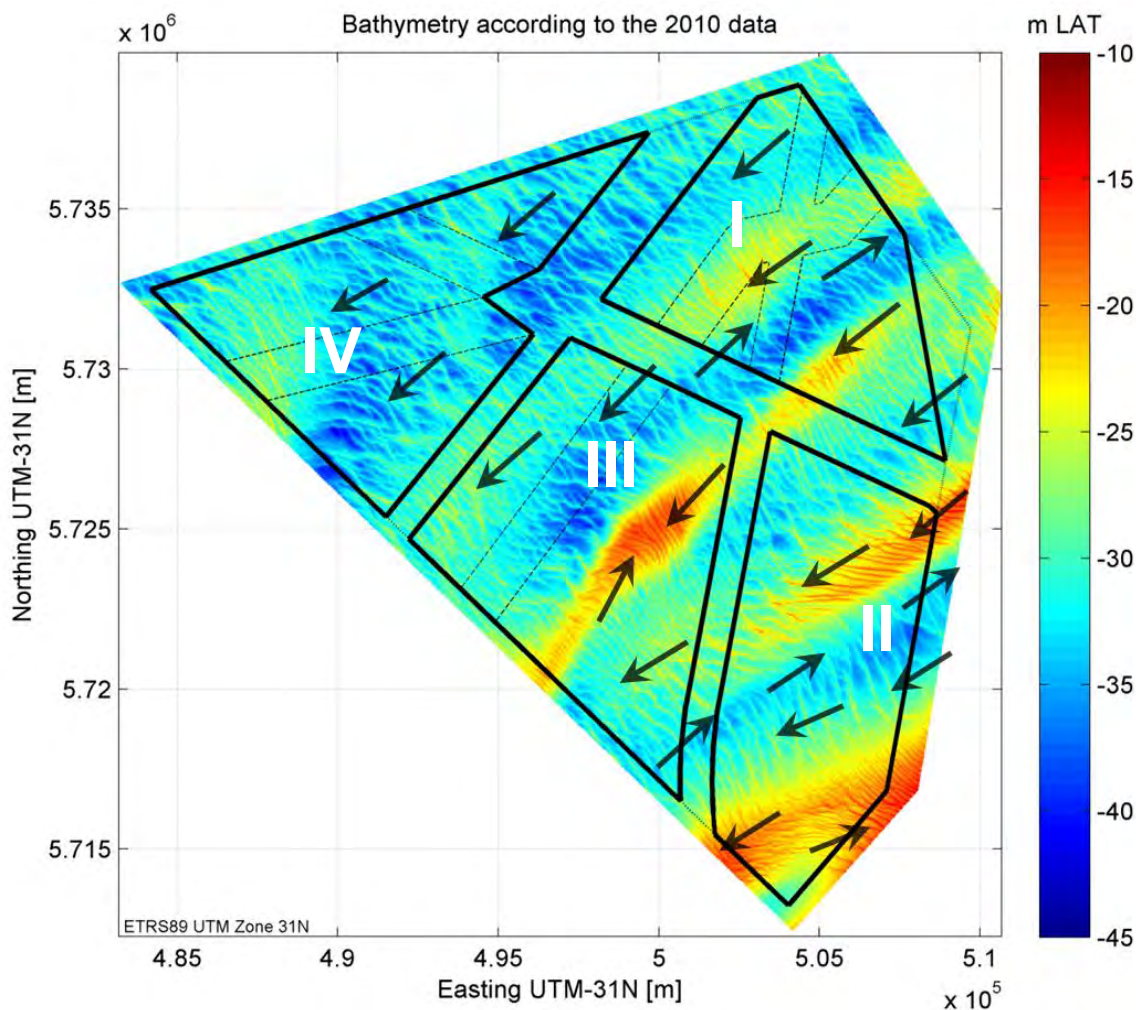


Figure 4.2 A schematized pattern of the sand wave migration directions on top of the BWFZ bathymetry.

4.3 Fourier analysis on individual bed forms

Following the determination of the bed form migration directions, a one-dimensional spectral analysis is used to determine individual sand wave dimensions and changes in time. The analysis is performed on transects that have to be drawn in the direction of sand wave migration to prevent that the migration velocity is underestimated. Differences in wavelength when not normal to the orientation of the crests are negligible. Similar to the determination of the migration directions, the Fourier analysis is also performed separately for the three distinct periods between the available surveys: 2000-2010, 2000-2015 and 2010-2015.

For all transects, crest and trough points of the individual sand waves are identified and tracked in time in the old and new Mobile Bathymetries of the considered period. Megaripples, which are superimposed on sand waves, are more dynamic than sand waves and are removed in the analysis to ensure consistent tracking of the crest and trough points. By truncating the high frequencies from a Fourier series that describes the bathymetric signal, the smaller megaripples are separated from the sand wave signal (Van Dijk et al., 2008). The megaripples are separated from the Mobile Bathymetry separately in the Fourier analysis, instead of using the Sand Wave Field, from which the megaripple information also was removed; the required cut-off wave length that produced the most accurate results in the Fourier analysis was determined in an iterative process and does not necessarily produce the same bathymetry as the Sand Wave Field.

From the filtered sand wave signal, crest and trough points are used to determine the wave lengths and wave heights of individual sand waves. By means of tracking these points in both surveys of the considered period, the migration rates of individual sand waves can be estimated. Figure 4.3 and Figure 4.4 below provide examples of two transects (of the 2010-2015 period) in which the sand waves move in opposite directions, illustrating the highly dynamic behaviour of the system:

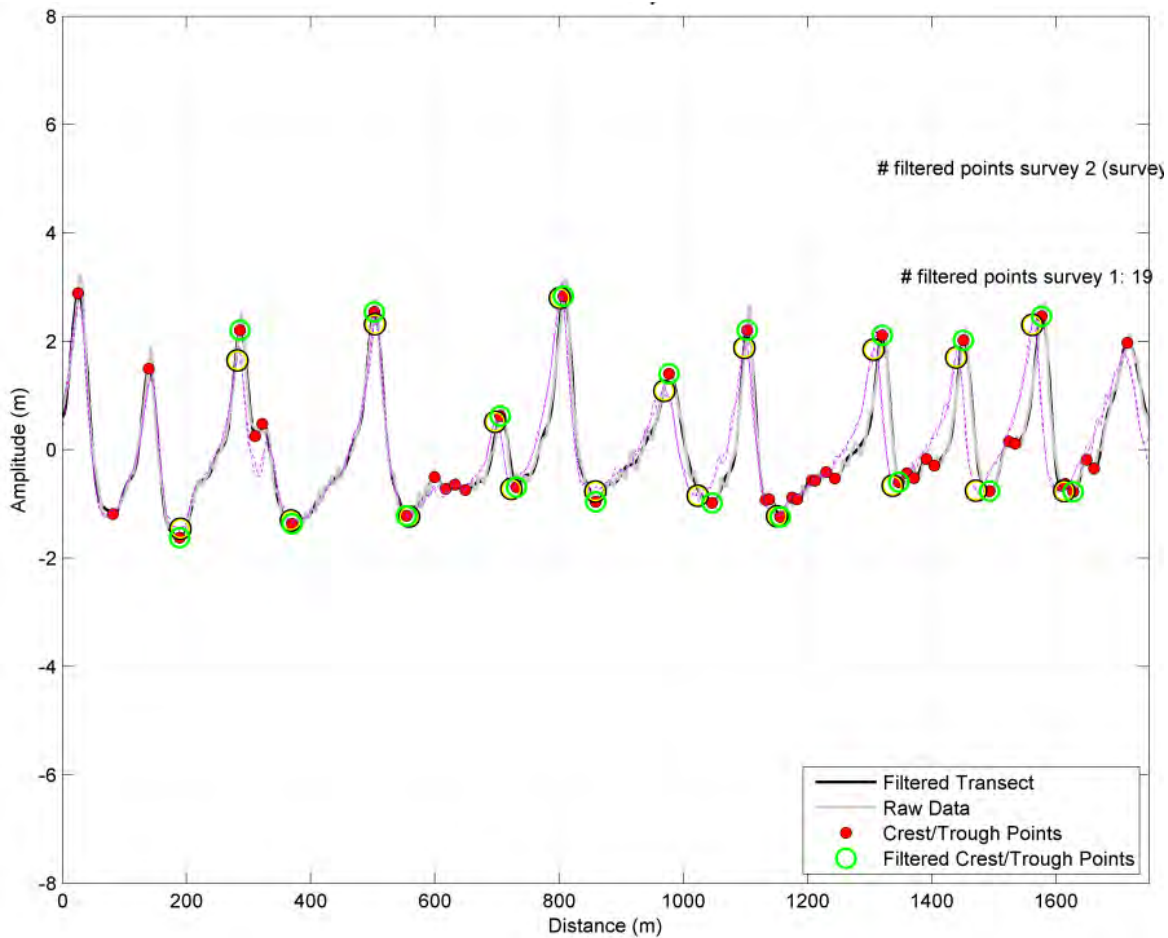


Figure 4.3 Example of Fourier analysis on one of the 1750 meter long transects from NE (left) to SW . Purple dashed line = sand wave signal based on 2010-bathymetrical survey; Pink dashed line = Fourier approximation of 2010 sand wave signal; grey solid line = sand wave signal based on 2015-bathymetrical survey; Black solid line = Fourier approximation of 2015 sand wave signal. The filled red dots indicate all crest/trough points and the green dots indicate which points have been selected for analysis (automatically or manually corrected) in the 2015-signal. Points selected in the 2010-signal are indicated by black circles. The plot shows a migration to the right, corresponding to the dominant SW-direction.

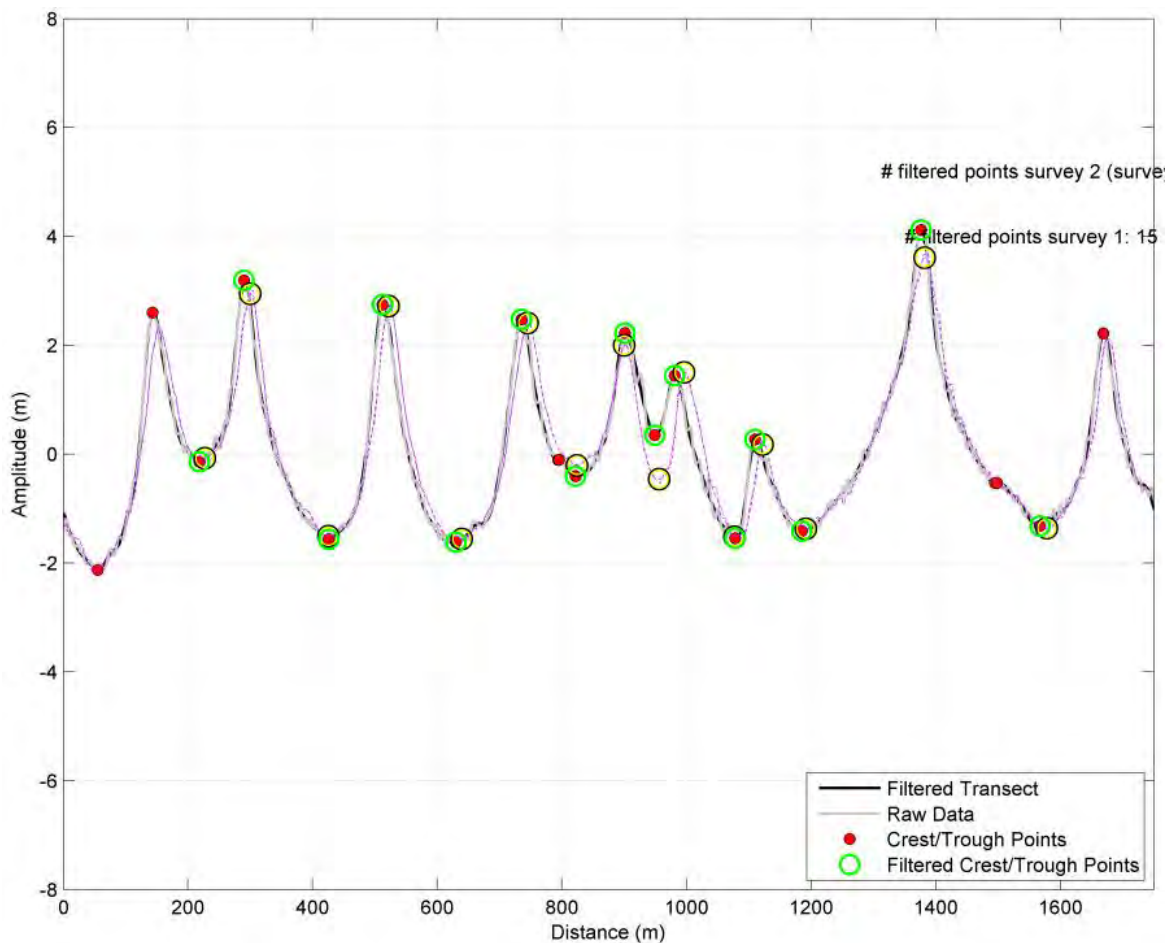


Figure 4.4 Example of Fourier analysis on one of the 1750 meter long transects from NE (left) to SW. Purple dashed line = sand wave signal based on 2010-bathymetrical survey; Pink dashed line = Fourier approximation of 2010 sand wave signal; grey solid line = sand wave signal based on 2015-bathymetrical survey; Black solid line = Fourier approximation of 2015 sand wave signal. The filled red dots indicate all crest/trough points and the green dots indicate which points have been selected (automatically or manually corrected) in the 2015-signal. Points selected in the 2010 survey are indicated by black circles. The plot shows a migration to the left, corresponding to the NE-direction.

Over the analysed transects, there is spatial variation in the sand wave displacement between surveys, i.e. not all sand waves and certainly not all selected crest and trough points, shift the same amount between surveys. Additionally, the three surveys were collected over a certain period of months to years; for instance, the various bathymetrical datasets that make up the 2000 bathymetry have been collected over a period of around 3 years in between 1999 and 2001 (see Section 2.2). To arrive at estimates of the annual migration rates, the migration distances derived from all selected crest and trough points have been divided by the time in between the surveys of the considered period. For each bathymetrical dataset, a suitable date was chosen within the period that the data was collected. The three datasets that make up the 2000 bathymetry have all been assigned a separate date.

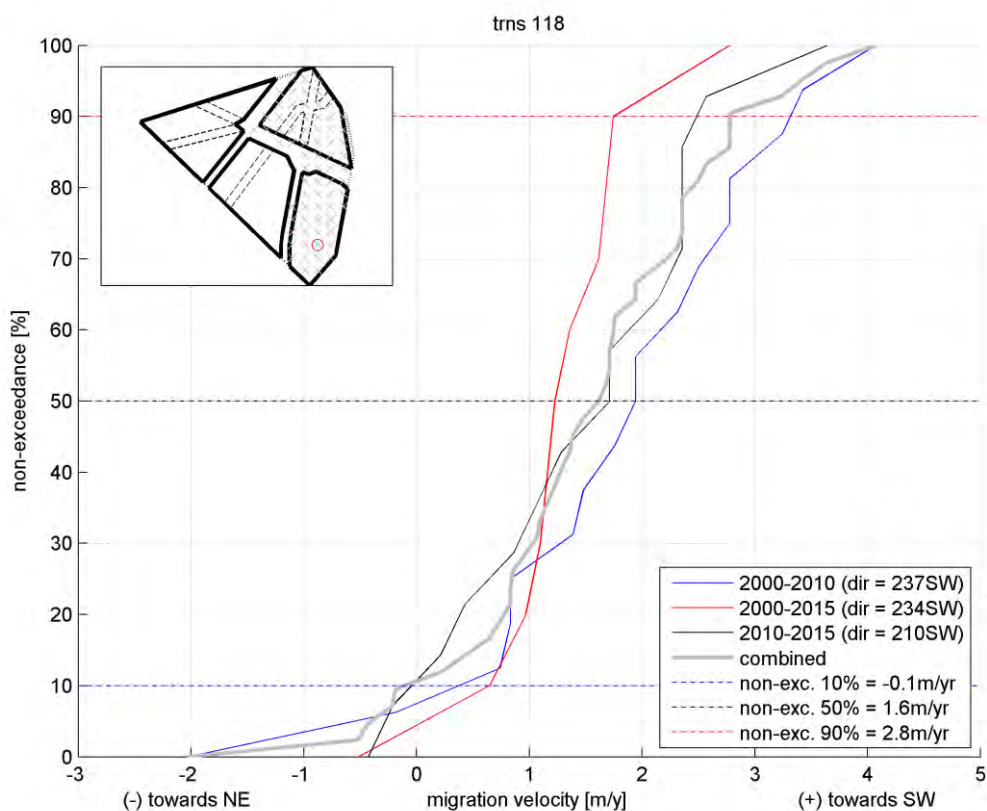


Figure 4.5 Example of results of Fourier analysis for transect 118 in WFS-II.

Figure 4.5 shows the results of the Fourier analysis for one of the 153 transects that were used to determine the migration velocities. In this non-exceedance plot, for each of the three considered periods (2000-2010 solid blue line, 2000-2015 solid red line, 2010-2015 solid black line), the estimated migration velocities are displayed of the individual selected crest and trough points. Note that not necessarily the same number of points is selected in the three periods. The considered migration direction for each period, following from the analysis described in the previous Section 4.2 is mentioned in the legend. The results of all three periods were combined in the thick solid grey line; the separate values of each period were merged, sorted and plotted together. Therefore, the values of each period were given an equal weight in the analysis. In the predictions of the future bathymetries and bed level changes, three migration velocities were taken into account from the combined line: the 10%, 50% and 90% non-exceedance values (respectively the dashed blue, black and red lines).

4.3.1 Sand wave statistics of the Borssele wind farm zone

The sand wave statistics are presented for the entire BWFZ (site I&II combined) and separately for WFS-I and II (see Figure 2.7 and Figure 2.8) for the period 2010-2015. Estimates are provided of the sand wave migration distances, migration speeds, wave lengths and wave heights in the form of maps and non-exceedance plots. The non-exceedance plots display the migration distances and corresponding migration speeds from individual crest and trough points and wave lengths and heights from individual waves. The maps display values averaged per transect.

The statistics are based on the tracking in time and space of selected crest and trough points. The selection of the crest and trough points in all surveys has been performed twice; once automatically on 665 transects (see top plot Figure 4.1) and once semi-automatically with manual correction wherever necessary on 153 transects spread further apart (see bottom plot of Figure 4.1). The manual inspection of the 153 transects was required to ensure that an equal amount of consistent crests and troughs were selected in both transects for each considered period; extinction and generation of sand waves prohibited a fully automated selection of these points. From these manually selected crest and trough points, the migration distances and velocities were calculated. The statistics of the wave lengths and heights have been derived from the automated tracking of the crest and trough points in the most recent survey in each considered time period on 665 transects, to ensure a sufficient data coverage.

Values for the migration distance and migration speed, averaged per transect and estimated using the manually selected crest and trough points of 153 transects, are presented in Figure 4.6 for the period 2010-2015. The migration directions show a reasonable comparison with Figure 4.1 in which the migration directions are highlighted in black (SW) and purple (NE). Note however, that the algorithm used to determine the migration directions in that figure has been optimized to find the migration directions and not the migration distances and therefore, differences can occur. Furthermore, the results presented in Figure 4.1 correspond to the 2000-2010 period. Also note that depending on which period is taken into account (2000-2010, 2000-2015 or 2010-2015), differences are found in migration directions, velocities, wave lengths and wave heights.

The 10% and 90% non-exceedance values (see Figure 4.7) show migration distances in between 8 meters in NE-direction and 9 meters in the dominant SW-direction with corresponding speeds of 1.7 meters per year in NE-direction and 1.9 meters per year in SW-direction (see Table 4.1). Generally speaking, the highest velocities are found on the crests and the lowest velocities in the troughs of the sandbanks of the underlying Static Bathymetry.

Parameter	10% non-exceedance	50% non-exceedance	90% non-exceedance
Migration distance [m]	-8	-1	9
Migration speed [m/yr]	-1.7	-0.2	1.9

Table 4.1 Sand wave migration statistics in the BWFZ, WFS-I&II combined, period 2010-2015 (- = NE, + = SW).

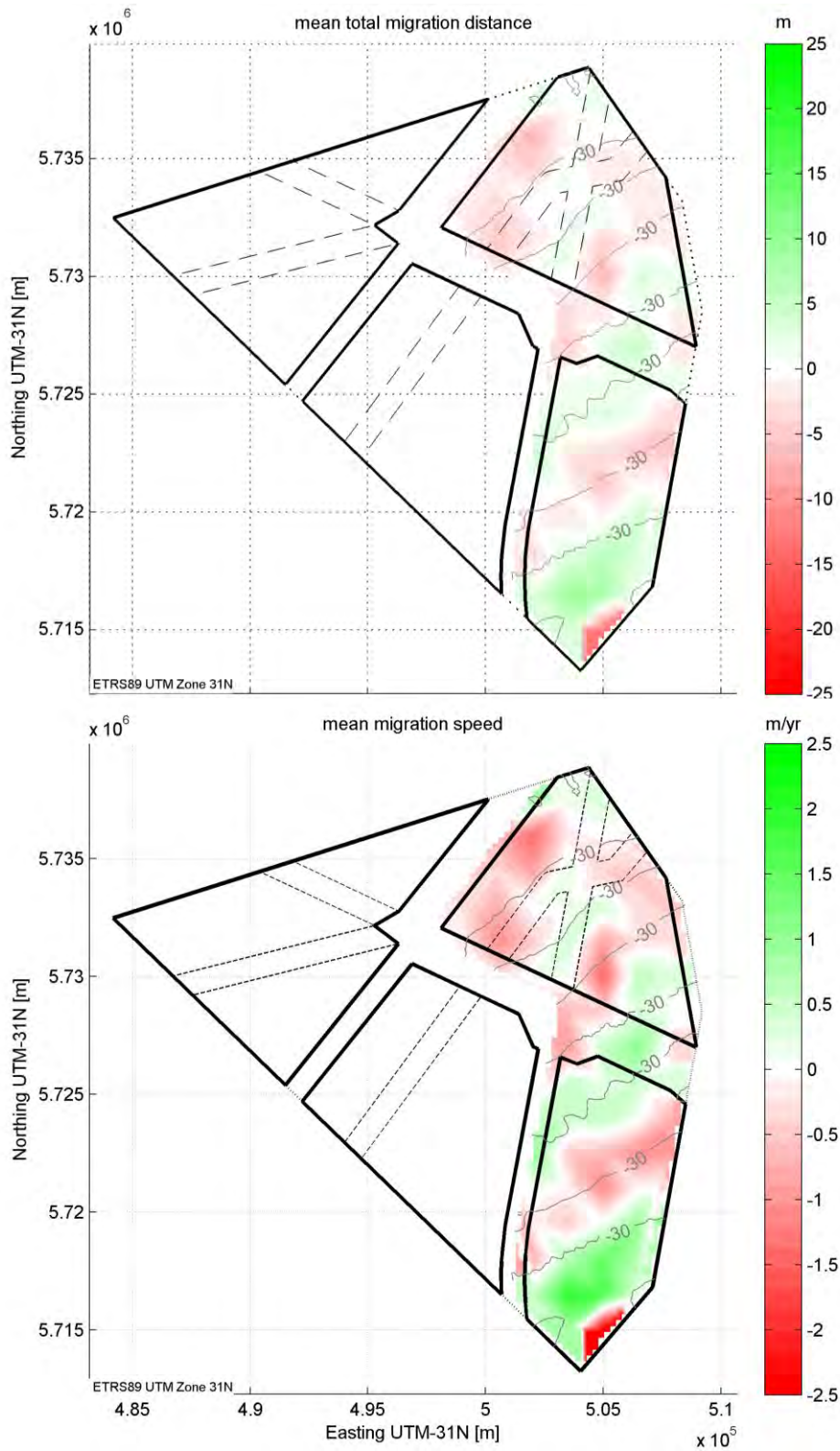


Figure 4.6 Site I&II: Maps of migration distances (top plot), migration speeds (bottom plot) estimated using the manual selection of crest/trough points of 153 transects for period 2000-2015 (red = NE, green = SW).

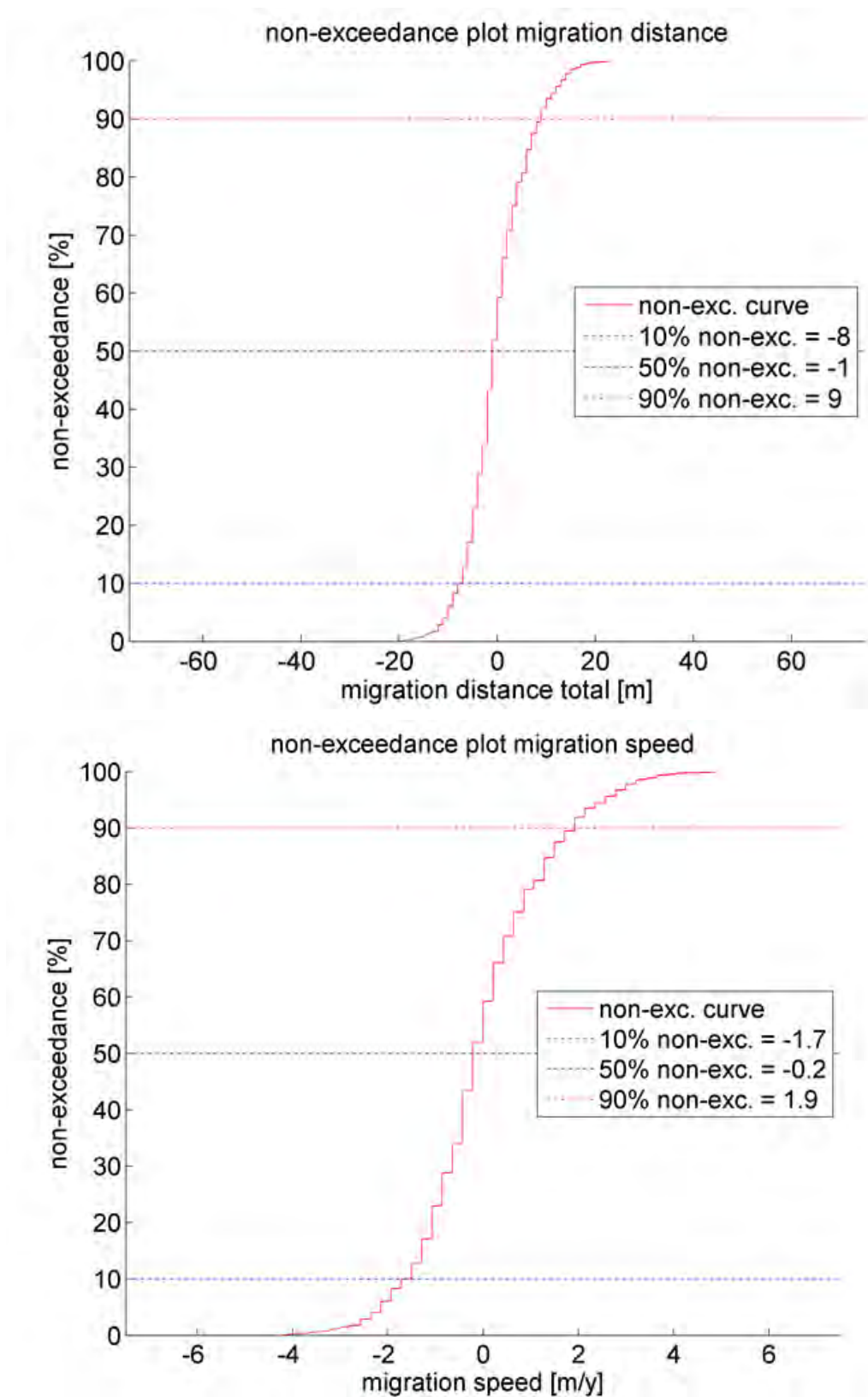


Figure 4.7 WFS-I&II: Non-exceedance plots of migration distances (top plot) and migration speeds (bottom plot) estimated using the manual selection of crest and trough points of 153 transects for period 2010-2015.

Figure 4.8 shows map plots of the estimated, transect-averaged, wave lengths (top plot) and wave heights (bottom plot) from the 2015 survey. These values are obtained using the automatically selected crest and trough points from the 665 transects displayed in the top plot of Figure 4.1 (note that the directions for the period 2000-2010 differ from the directions found in the period 2010-2015). Overall, low, short waves are found on the crests and longer, higher waves in the troughs of the sandbanks of the underlying Static Bathymetry. This behaviour is expected since sand waves can only grow to a certain percentage of the water depth (e.g. Yalin, 1964). Although these results have a higher resolution, the results are also in line with the results of Van Alphen and Damoiseaux (1989), see Figure 2.9. Figure 4.9 shows the non-exceedance plots of both wave length and wave height. The values of 10%, 50% and 90% non-exceedance are summarized in Table 4.2 below:

Parameter	10% non-exceedance (2010/2015)	50% non-exceedance (2010/2015)	90% non-exceedance (2010/2015)
Sand wave length [m]	134/132	239/236	433/422
Sand wave height [m]	1.9/1.9	3.6/3.7	5.9/5.9

Table 4.2 Sand wave characteristics for WFS-I&II combined for the period 2010-2015.

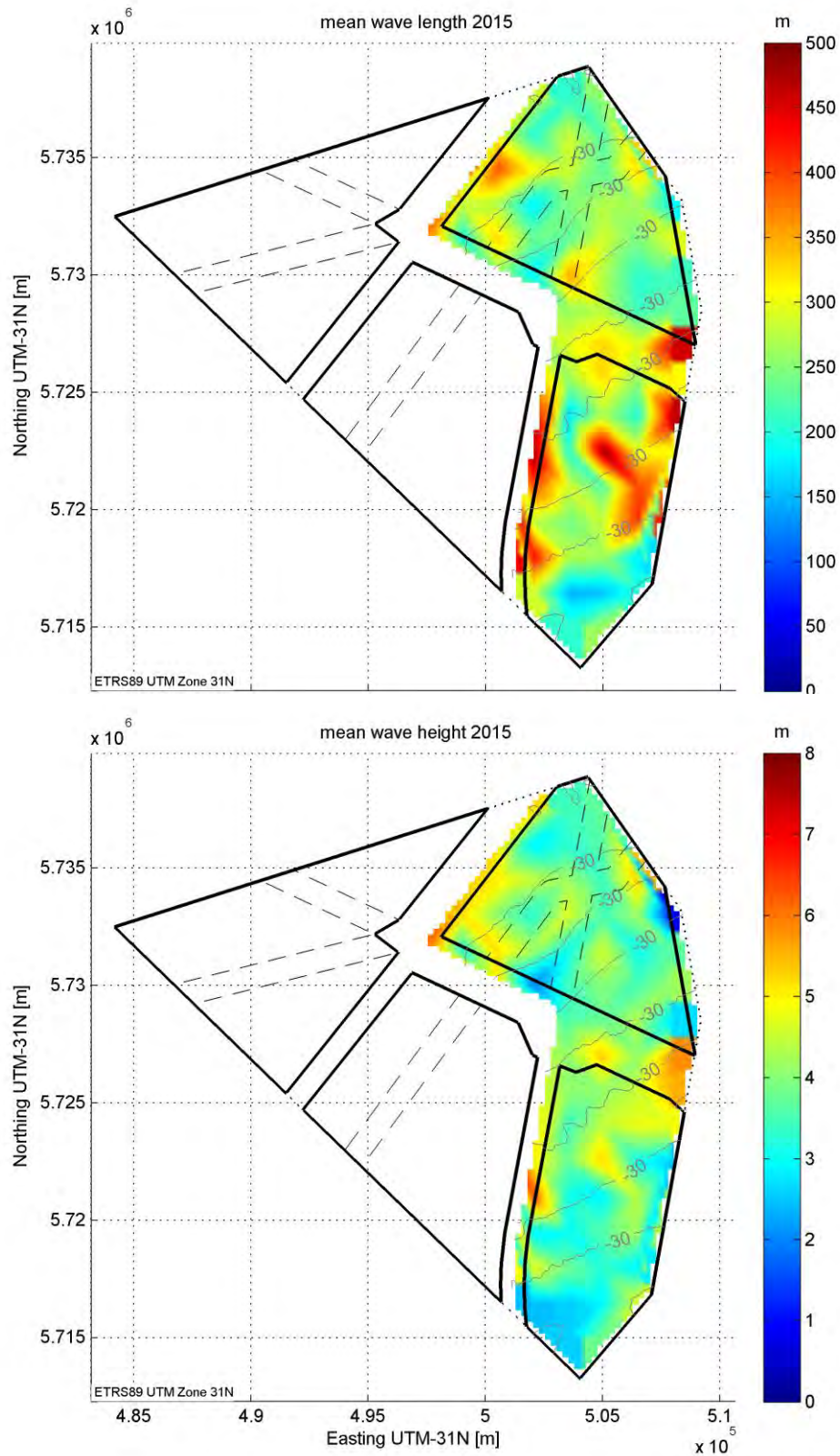


Figure 4.8 Site I&II: Map plots of wave lengths (top plot) and wave heights (bottom plot) estimated using the automatic selection of crest and trough points of 665 transects for the 2015 survey.

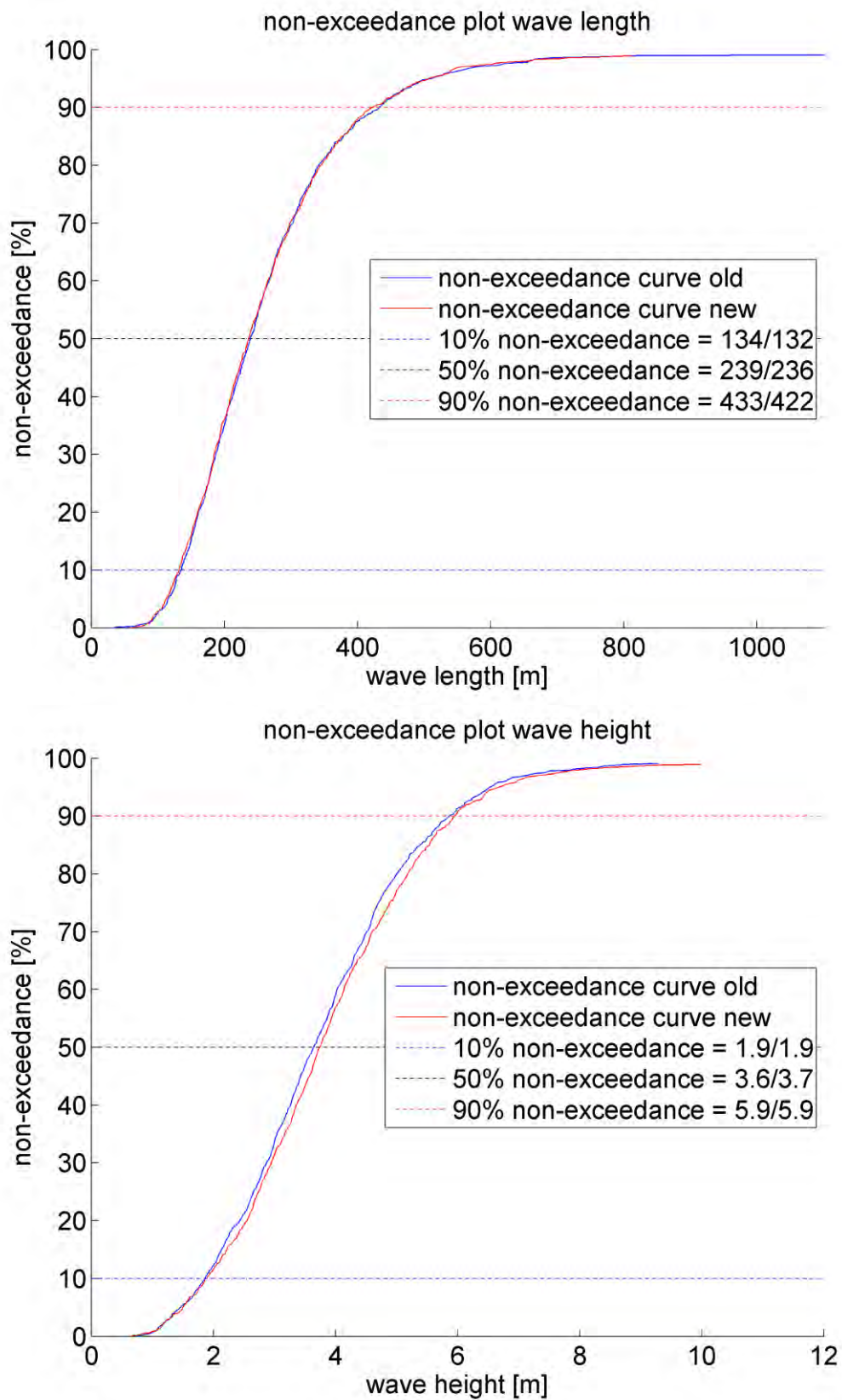


Figure 4.9 Site I&II: Non-exceedance plots of wave lengths (top plot) and wave heights (bottom plot) estimated using the automatic selection of crest and trough points of 665 transects (period 2010-2015).

4.3.2 Sand wave statistics per site

Per site, four non exceedance plots are presented of migration distance, migration speed, sand wave length and sand wave height for the period 2010-2015. Note that, given the 1750 meter long transects used, all waves within the sites, including sand waves in the safety zones have been taken into account.

Statistics of sand waves in WFS-I

In WFS-I, in the period 2010-2015, sand waves are migrating in both south-western and north-eastern direction. The migration speeds are relatively low, ranging between a 10% non-exceedance value of 1.7m/s in north-eastern and a 90% non-exceedance value of 1.5 m/s in south-western direction. The sand wave characteristics of the site are presented below in Table 4.3 and Figure 4.10.

Parameter	10% non-exceedance (2010/2015)	50% non-exceedance (2010/2015)	90% non-exceedance (2010/2015)
Migration distance [m]	-8	-2	7
Migration speed [m/yr]	-1.7	-0.4	1.5
Wave length [m]	141/133	236/228	391/387
Wave height [m]	2.1/2	3.9/3.9	5.7/5.9

Table 4.3 Sand wave characteristics of WFS-I (migration distance/speed: negative values towards northeast, positive values towards southwest).

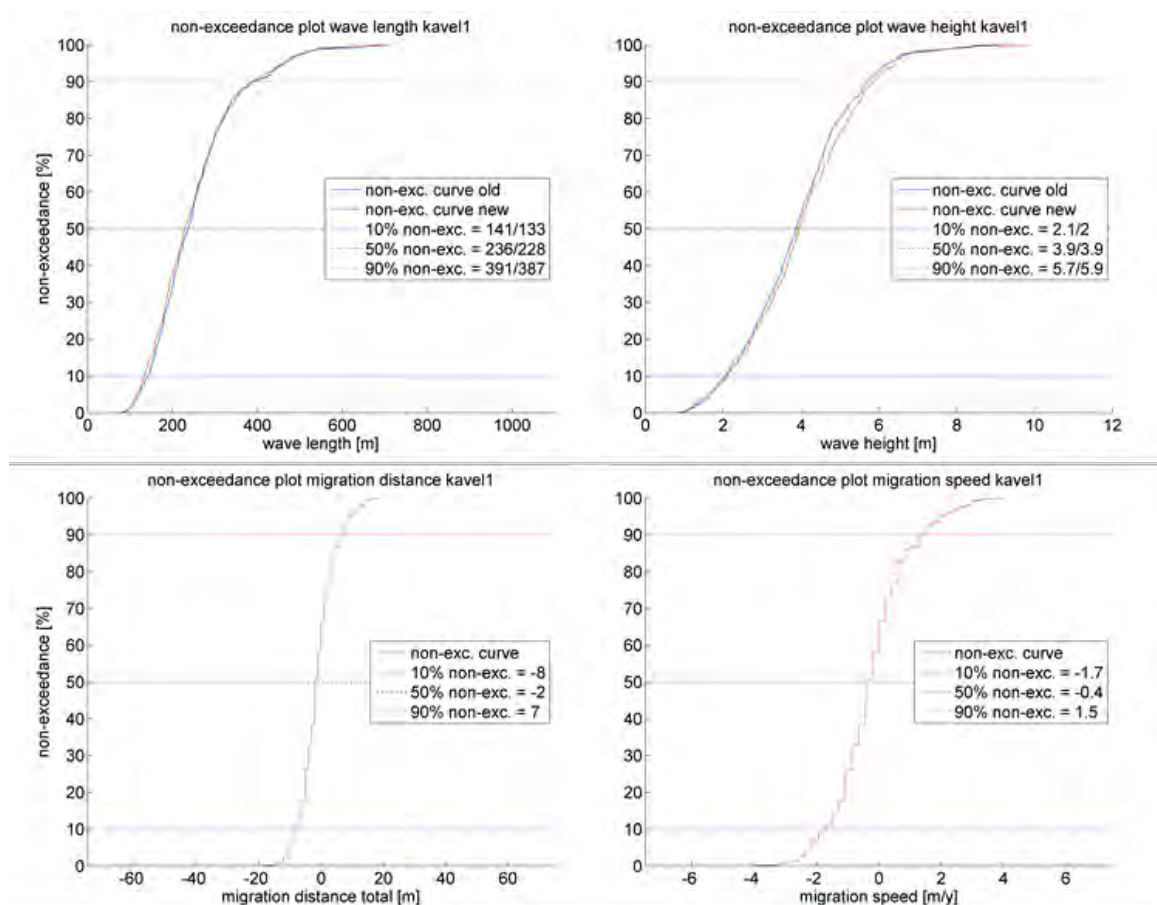


Figure 4.10 Sand wave characteristics of WFS-I.

Statistics of sand waves in WFS-II

From Figure 4.6, it becomes clear that in the period 2010-2015, WFS-II is divided in three clear parts of alternating sand wave migration direction; the northern top part migrates relatively slowly in the governing south-western direction, the middle part moves relatively fast to the northeast (given that the north-eastern-directed migration is generally slower than the south-western-directed migration) and the southern part moves fast to the southwest. In this last part, located on the crest of an underlying sandbank, the largest migration rates are found of the entire BWFZ. The sand wave characteristics of the site are displayed below in Table 4.4 and Figure 4.11.

Parameter	10% non-exceedance (2010-2015)	50% non-exceedance (2010-2015)	90% non-exceedance (2010-2015)
Migration distance [m]	-8	1	10
Migration speed [m/yr]	-1.7	0.2	2.1
Wave length [m]	124/122	241/242	455/450
Wave height [m]	1.5/1.6	3.2/3.3	5.7/5.7

Table 4.4 Sand wave characteristics of WFS-II (migration distance/speed: negative values towards northeast, positive values towards southwest).

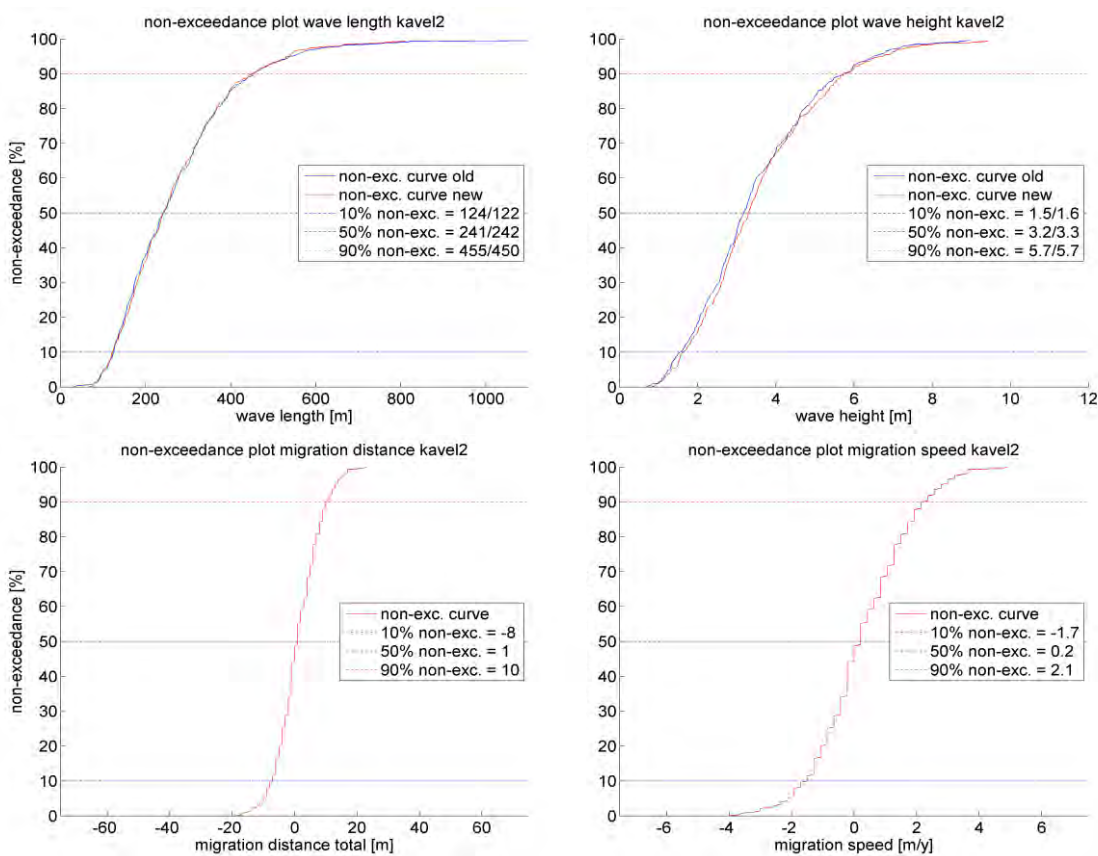


Figure 4.11 Sand wave characteristics of WFS-II.

5 Prediction of future bathymetries and bed level changes

5.1 Introduction

This chapter discusses the methodology and presents the results of the predictions of future bathymetries and the corresponding bed level changes. The chapter starts with a description of the various sources of uncertainty in Section 5.2. Following these uncertainties, a suitable uncertainty band is determined. In Section 5.3, the methodology of predicting the future bathymetries is presented. In Sections 5.4 and 5.5, these future bathymetries are used to determine the Reference SeaBed Level (RSBL) and Maximum SeaBed Level (MSBL). Furthermore, the corresponding bed level changes relative to the 2015 bathymetry are predicted. In Section 5.6, the RSBL is validated against the base of the Holocene formations. In the final section of this chapter, Section 5.7, the RSBL and MSBL and the corresponding predicted seabed level lowering and rising are translated into indicative recommendation zones for foundations and electricity cables.

5.2 Sources for uncertainty

In the prediction of the future bed level changes and corresponding bathymetries, various sources of uncertainty have to be taken into account. The main sources of uncertainty in a data-driven morphological analysis based on measured bathymetrical data are:

- i) Uncertainty due to data collection and differences in the collection of data
- ii) Uncertainty in the pre-processing of data
- iii) Uncertainty in the methodology of analysis and prediction

(i): The datasets that have been used in this study are either collected by means of single beam echo sounding (SBES; 2000 combined dataset) or multi beam echo sounding (MBES; 2010 and 2015 datasets). MBES data are more accurate than SBES data. One of the reasons is the shoal-biased nature of SBES; this biasing is caused by the fact that SBES measures the first return of the echo sounding. For example, when megaripples occur, the crest of the megaripple within the SBES beam width determines the measured water depth. For MBES, the separate beams also register the troughs of the megaripples. Uncertainties are however still present when using MBES data; for instance, the data becomes less accurate further away from the ship where the angle between the seabed and the echo sounding device on the ship increases.

(ii): After collection of the bathymetrical data, the raw echo sounding signals are processed before they can be applied in further analysis. Typical examples of such pre-processing are corrections for the movement of the ship during the measurements and tidal reduction; correcting for the tidal signal, depending on the local position of the ship during the measurement time interval. Different methods of tidal reduction can result in relative large vertical differences between surveys in time. Furthermore, the data are typically gridded to a raster of data points with a fixed resolution in x- and y-direction; the raw data are interpolated to a fixed grid. The number of data points within each grid cell is dependent on the resolution of the data and the resolution of the grid. The value of a grid cell is determined by taking the minimum, maximum, mean or another statistical value of all raw data points in the cell. In more recent MBES data, delivered on high resolution grids (2015 DEEP data on a 1x1m grid), this is of less importance.

(iii): The last mentioned source for uncertainty in the data are due to the applied analysis methods. As mentioned in Section 4.3, the exact timing of the measurements of individual

data points in the various surveys is not known; there is a certain period in which the surveys are collected. This leads to an uncertainty of the estimates of the sand wave migration velocities. Furthermore, to arrive at future seabed predictions, the 2015 data is migrated using different migration directions and velocities (see Section 5.3 for further details). This approach assumes that the seabed is in a state of dynamic equilibrium, which implies that the sand waves will retain their shape and dimensions while they are migrating. However, as stated earlier, the Borssele wind farm zone is highly dynamic with opposing sand wave migration directions and (observed in some transects) generation and extinction of sand waves. Furthermore, event-driven changes of the sand wave shape (e.g. during storms) and seasonal changes may occur (see Section 2.6).

The various sources of uncertainty have to be accounted for in the results by applying an uncertainty band. The uncertainty band that is applied in the analysis consists of three separate contributions:

- Uncertainty band due to the survey inaccuracies
- Uncertainty band due to existence of megaripples
- Uncertainty band to account for the assumption of shape retaining sand waves

Note that the uncertainty band is applied both upward and downward; the upward and downward bands do not necessarily have the same amplitude.

The uncertainty band due to the survey inaccuracies was determined by analyzing the uncertainty reported by DEEP (bathymetry uncertainty grid, 95% confidence, at 1m resolution) in the 2015 geophysical investigations. This dataset contains the survey uncertainty per measured data point. Note that it is not reported how these uncertainty values were calculated. As no clear trend was visible in the spatial distribution of this uncertainty, all data was plotted in a non-exceedance curve, both per site and for the two sites combined. From this curve, the 95% non-exceedance value of 0.20m is applied in the uncertainty band, both upward and downward. This uncertainty band captures the sources of uncertainty mentioned under points (i) and point (ii). As the 2015 MBES data was used in the predictions of the future seabed levels, the additional uncertainties because of the use of the 2000 SBES do not have to be accounted for separately.

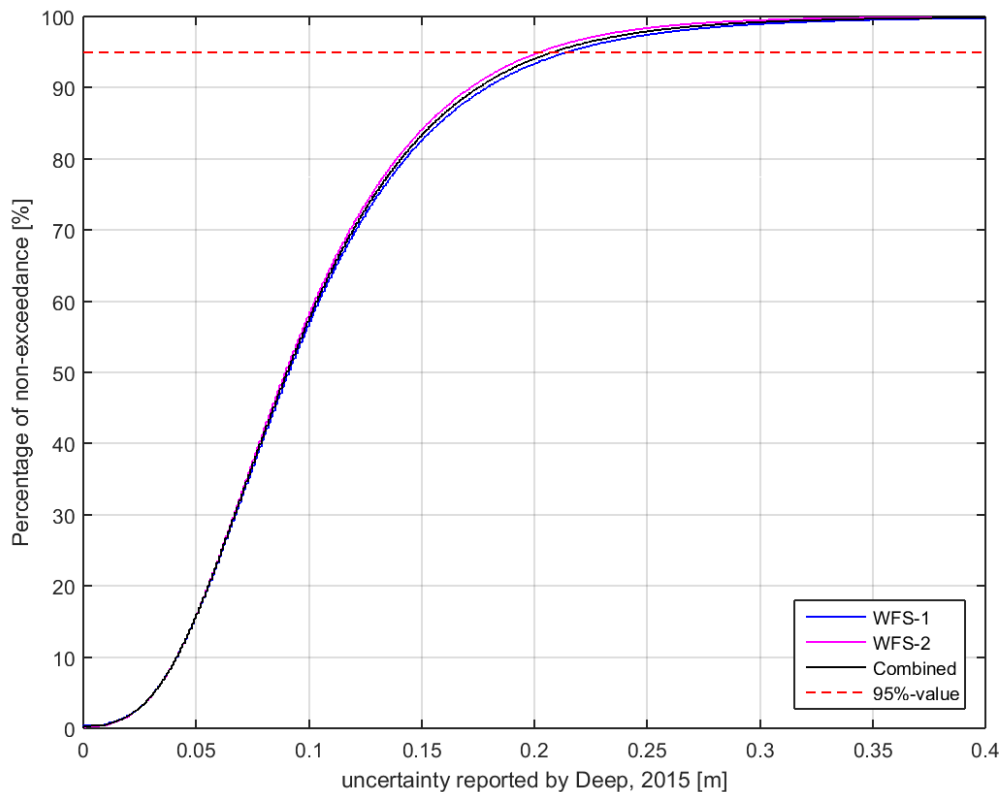


Figure 5.1 Non-exceedance plot of the uncertainty reported by DEEP, 2015 (source: 20150327_SDB_DEEP_WFS1_MBE-uncertainty_1x1_V01_F.xyz, 20150327_SDB_DEEP_WFS2_MBE-uncertainty_1x1_V01_F.xyz).

The second source to include in the uncertainty band is the uncertainty due to the existence of megaripples. As described in Section 3.3, megaripples have migration speeds that are so large that many megaripples will pass at each foundation throughout the lifetime of wind farms. Therefore, it was decided not to predict the migration of the megaripples, but to analyse the megaripple field and include some representative statistical values in the uncertainty band. The 95% non-exceedance values of respectively the megaripple troughs and heights that are applied in the uncertainty band are 0.4m downward and 0.6m upward.

The third contribution to the uncertainty band is the assumption of shape retaining sand waves. In Section 2.6, a detailed description is presented of the physical processes behind sand waves. The conclusions of this section are that sand waves remain more or less similar over decades, but (temporary) seasonal changes may occur, mainly related to the occurrence of severe storms. In the predictions of future bed level changes, a rather wide range of migration directions (3 different directions) and migration velocities (10-90%) is applied, which is considered to result in a sufficiently wide range of predicted future seabed levels. It is assumed that by applying these ranges, the seasonal changes to sand wave shapes that are described in Section 2.6 and mentioned as source of uncertainty under (iii) are sufficiently accounted for. Therefore, no additional uncertainty was added to the uncertainty band.

The total uncertainty band that is applied on the predicted future bed level changes and corresponding bathymetry therefore becomes:

- Uncertainty band upward: 0.20m (survey uncertainty) + 0.6m (megaripple uncertainty) = +0.80m.

- Uncertainty band downward: -0.20m (survey uncertainty) - 0.4m (megaripple uncertainty)
= -0.60m.

5.3 Predicting future bathymetries and bed level changes in period 2015-2046

The various bathymetrical data fields that are used in this study are presented in Table 3.1. These data fields are the result of the large scale bathymetric filtering of the 2015 data. The future bathymetries and the corresponding bed level changes are estimated by artificial shifting of the mobile components of the most recent 2015 bathymetry but excluding the megaripple information; i.e. shifting of the Sand Wave Field. The megaripple information and other uncertainties are added later by applying the uncertainty band described in the previous paragraph.

For 153 transects, three distinct migration directions were computed corresponding to the three considered periods (2000-2010, 2000-2015, 2010-2015) between the three available surveys (see Section 4.2). Furthermore, for each transect, three distinct migration velocities were determined in the Fourier analysis, the 10%, 50% and 90% non-exceedance values (see Section 4.3). The considered period of 2015-2046 contains 31 years. For each year (timespan), for each distinct combination of migration direction and velocity, a map field of shifts in x- and y-direction was interpolated between the data points of the 153 transects. This led to 9 distinct migration fields for each considered year. The Sand Wave Field was then shifted according to these migration fields, leading to 9 distinct bathymetries for each year. For the total period of 31 years, this implies a total of $9 * 31 = 279$ distinct bathymetries. The 9 future bathymetries of each year are constructed by addition of the 9 migrated Sand Wave Fields (mobile component) to the Static Bathymetry (static component). Figure 5.2 displays an example of a predicted 2046 bathymetry corresponding to a distinct migration direction and velocity pair together with a difference plot between the predicted 2046 and the measured 2015 bathymetry. The difference plot clearly shows the migration direction and velocity of the Sand Wave Field.

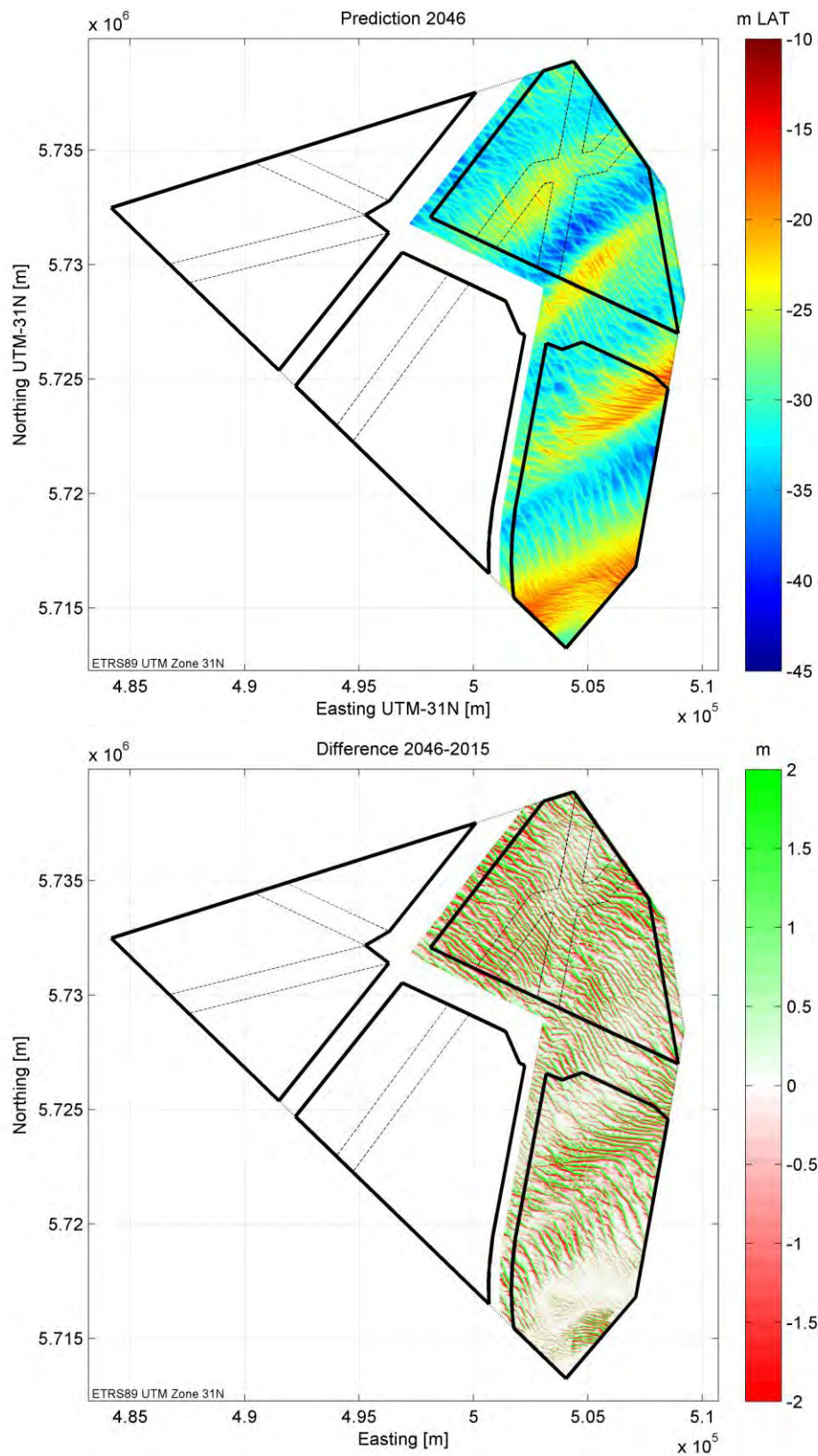


Figure 5.2 Top plot: Predicted bathymetry 2046 for one distinct pair of migration velocity and migration direction.
 Bottom Plot: Difference between the predicted 2046 and measured 2015 bathymetry.

In the next step, the total envelope of the mobile components of 2015 bathymetry was determined, using the 279 distinct migrated Sand Wave Fields. For each data point, from the stack of migrated Sand Wave Fields, the minimum and maximum values were determined. The minimum and maximum values correspond to respectively the lower envelope (Figure 5.3) and upper envelope (Figure 5.4) of the migrated Sand Wave Fields in the entire 31 year period.

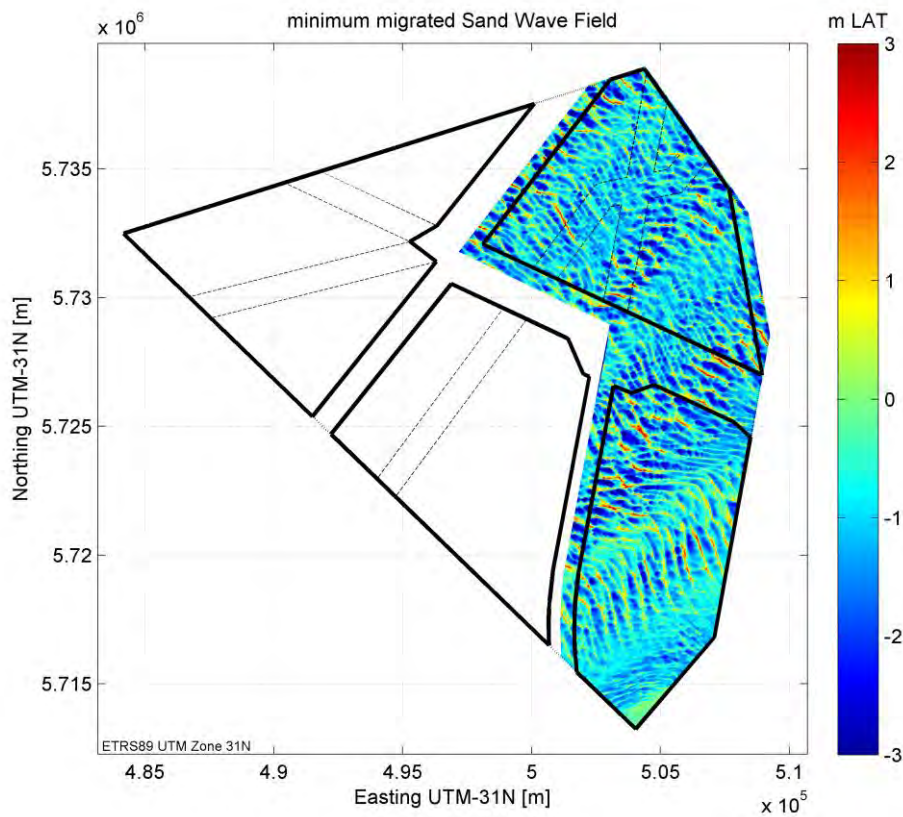


Figure 5.3 Lower envelope of the migrated Sand Wave Field for the entire 31 year period (2015-2046).

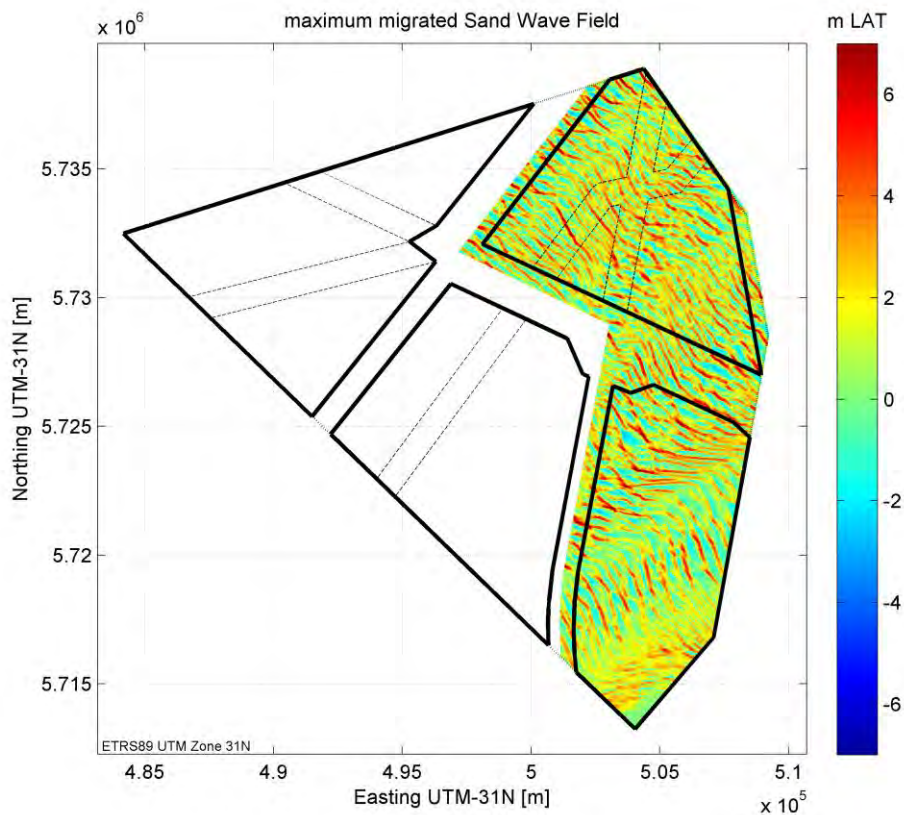


Figure 5.4 Upper envelope of the migrated Sand Wave Field for the entire 31 year period (2015-2046).

As expected, it can be observed from Figure 5.3 and Figure 5.4 that the highest values are found around the sand wave crests and lowest values around the sand wave troughs. Note that although the maximum and minimum values are displayed, negative values are still present in the upper envelope and positive values are still present in the lower envelope of the migrated Sand Wave Field. This is explained by the fact that the migrated Sand Wave Field still consists of both crests and troughs; the maximum around a trough and the minimum around a crest will therefore respectively still be negative and positive.

5.4 Reference SeaBed Level (RSBL)

Next, by combining the lower (mainly negative) envelope of the migrated Sand Wave Field (Figure 5.3) with the Static Bathymetry, the expected minimum seabed level in the lifetime of the wind farms is obtained. The RSBL is estimated by addition of the downward uncertainty band, discussed in Section 5.2. The result is presented in Figure 5.5. The overall bathymetry of the RSBL looks very similar to the static bathymetry, but it is typically a few meters deeper. The RSBL varies between -16.1m LAT and -40.3m LAT. The deepest parts are found in the flood channel in the middle of WFS-I.

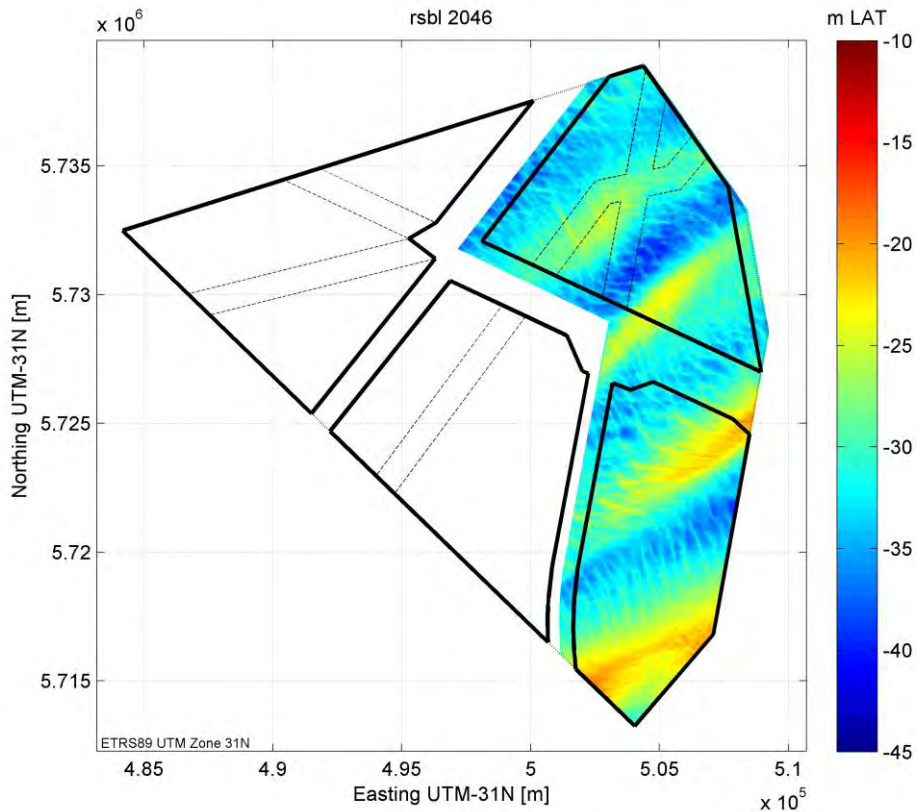


Figure 5.5 The Reference SeaBed Level (RSBL). The RSBL is the summation of the lower envelope of the migrated Sand Wave Field (Figure 5.3) and the Static Bathymetry (Figure 3.2 bottom middle), including the downward uncertainty band.

By calculating the difference between the RSBL and the most recent 2015 bathymetry, the maximum expected seabed level lowering can be predicted (Figure 5.6). It should be noted that the observed pattern follows the large-scale bed form geometry. The current crests of the sand waves have the largest predicted drop in seabed level, while the deepest troughs of the sand waves have a zero predicted drop (i.e. these are already at their lowest and will only experience a seabed level rise). This pattern is observed over the entire area, but on top of the underlying sandbanks the height variation between the crests and troughs is typically less, as the wave height typically decreases on these sandbank crests; higher sand waves are found in the swales between the sandbanks.

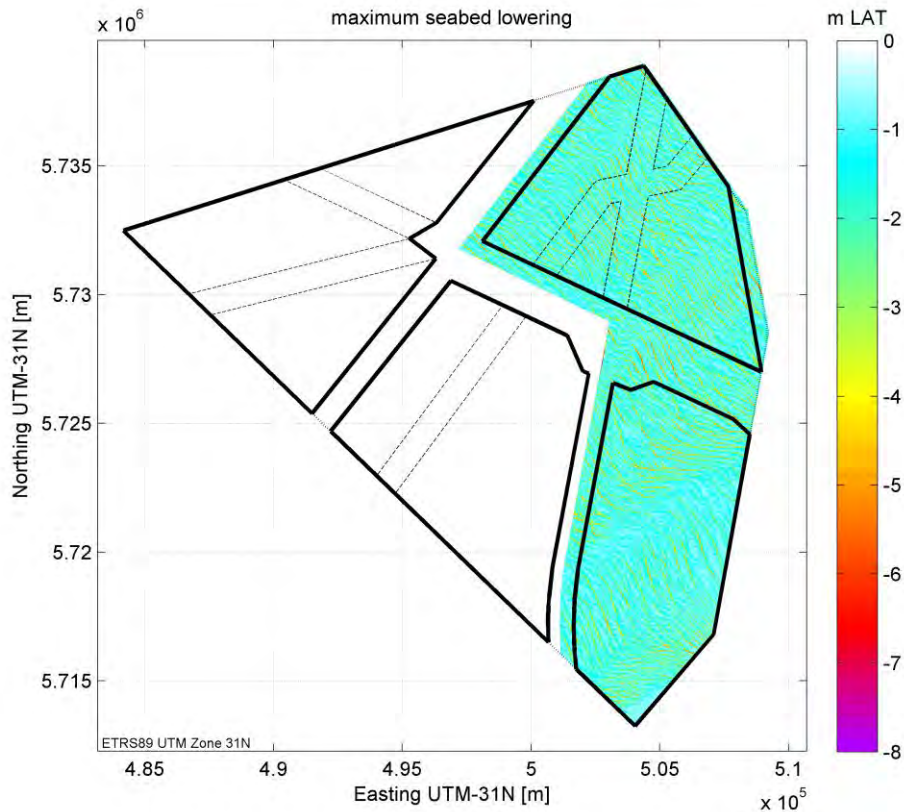


Figure 5.6 The maximum predicted seabed lowering based on the 2015 bathymetry. The values indicate the difference between the 2015 bathymetry (Figure 2.2) and the RSBL (Figure 5.5).

Note that at the boundaries, the results are less reliable due to lack of data. In the next phase, when the data of WFS-III and WFS-IV become available and are included in the analysis, this problem will no longer exist at the inner boundaries between WFS-I,II and WFS-III,IV. At the outer edges of WFS-I and WFS-II however this problem will remain; the surveyed area extends only a few tens of meters outside the site boundaries. When sand waves are migrating into the BWFZ-area, at some point in time, near the boundaries, no more data is available to migrate. Depending on the bathymetric features outside the edges, the total range in predictions can be too small because of the lack of data. The area that is potentially affected lies within 50m from the boundary of the surveyed area in 2015 and the potential changes to the RSBL (and also the MSBL, see next section) will be larger when being closer to the boundary.

5.5 Maximum SeaBed Level (MSBL)

Similar to the procedure to determine the RSBL, the Maximum SeaBed Level (MSBL) was determined. Now the upper (mainly positive) envelope of the migrated Sand Wave Field (Figure 5.4) was used. By combining the upper envelope with the Static Bathymetry (Figure 3.2 bottom middle) and adding the upward uncertainty band, the Maximum SeaBed Level (MSBL) is obtained. The MSBL is shown in Figure 5.7. The overall bathymetry of the MSBL looks very similar to the static bathymetry, but it is typically a few meters shallower. The MSBL varies between -13.3m and -38.2m LAT.

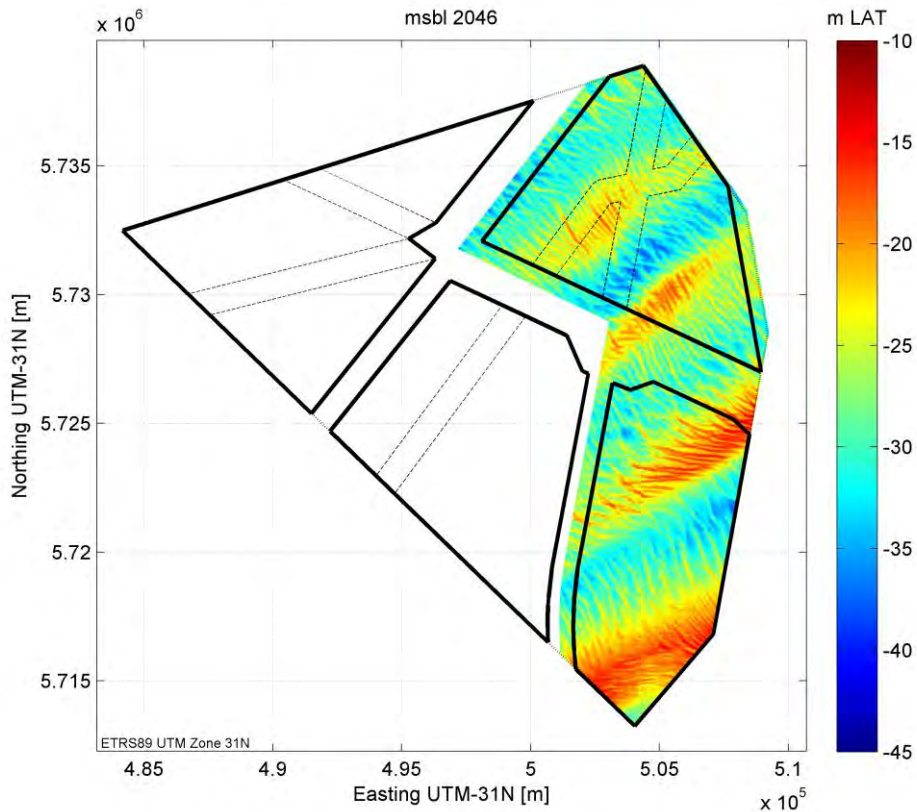


Figure 5.7 The Maximum SeaBed Level (MSBL). The MSBL is the summation of the upper envelope of the migrated Sand Wave Field (Figure 5.4) and the Static Bathymetry (Figure 3.2 bottom middle), including the upward uncertainty band.

By calculating the difference between the MSBL and the 2015 bathymetry, the maximum expected rise of the seabed can be predicted (Figure 5.8). The current sand wave troughs of the 2015 bathymetry have the largest predicted rise in seabed level, while the highest crests of the sand waves have a zero predicted rise. Note that the seabed close to the foundations will most likely not rise significantly, because local scour will counteract this. Buried electricity cables that cause no flow disturbance themselves will obviously not have this “beneficial” scour effect and therefore will experience a rising seabed if a sand wave crest passes over. This might be relevant for the maximum cable temperature (“thermal bottleneck effect”).

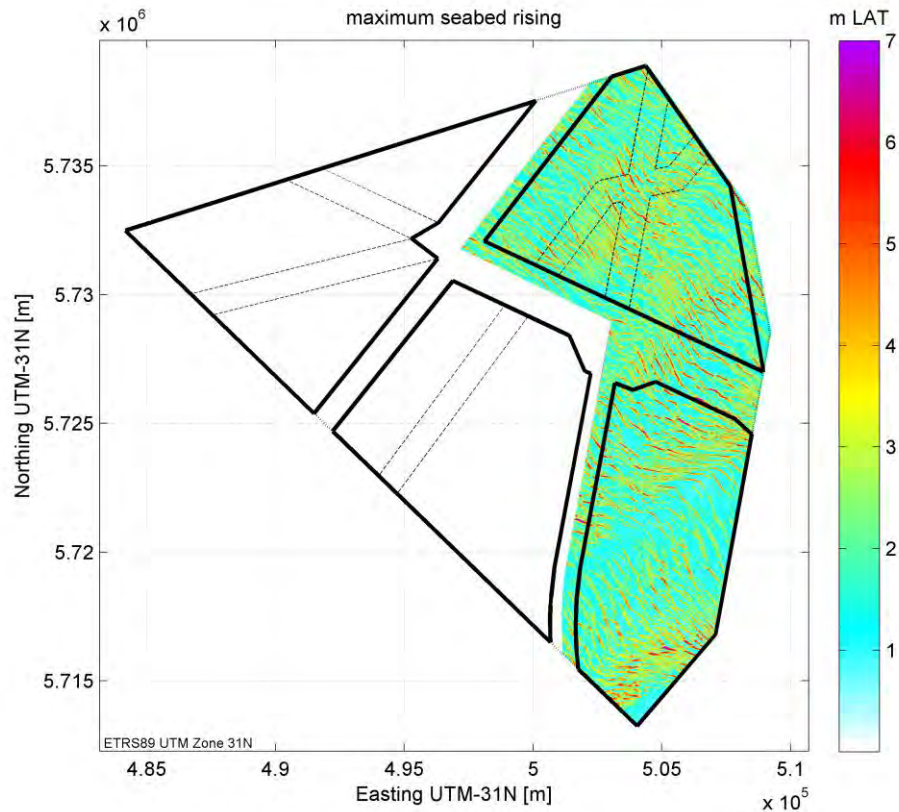


Figure 5.8 The maximum predicted seabed rising based on the 2015 bathymetry. The values indicate the difference between the 2015 bathymetry (Figure 2.2) and the MSBL (Figure 5.7).

5.6 Comparison of RSBL with base of Holocene formations

The morphodynamic bed level changes all take place in the Bligh Bank Formation and Buitenbank Formation, which both consist of marine sands and were deposited in the Holocene. This geological/seismic unit was named U7 in the geophysical site investigation by Deep (2015a, 2015b). The description of this unit as described by Deep is provided in the text box below.

(p64 of Deep, 2015a and 2015b)

Seismic unit U7 is identified throughout the entire area with both SBP and MCS surveys and corresponds to the Holocene Buitenbanken and Bligh Bank Formations. These are made up of sands that make up the complex geomorphology observed at the sea bed. The lower boundary of U7 is a fairly planar surface and it lies on top of seismic unit Pleistocene deposits (U6), or Tertiary units on U4 or U5 when the Pleistocene cover is not present. The basal unit is of an erosive nature, in some areas possibly corresponding to a paleo-topography. The upper limit for this unit is the seafloor itself since it is the youngest unit in the BWFZ.

The base sits between depths of around 20 to 40m below LAT. The thickness of this unit varies between less than a meter to about 17 meters. Since the base is relatively planar, the highest thickness values are found where the seafloor rises, on top of the sandbanks.

When this unit overlies the Tertiary deposits (U4 or U5) a clear unconformity is identified. Where it overlies the Pleistocene unit (U6) usually a clear horizon is identifiable. However, because the underlying deposits rarely have an internal structure, the unconformity associated with the erosive nature of the base is not clear.

...

Interpretation of the SBP survey data has revealed the base of seismic unit U7 very consistently throughout the survey area. Nonetheless, underneath the sandbanks the penetration of the SBP seismic signal was not sufficient to identify the base of U7.

...

From cross-correlation between the MCS and SBP interpretation results it was shown that there was good overlap between the data sets. The isopach maps of U7 from both surveys showed that the modelled thicknesses correlated very well.

Although it is not certain whether the underlying deposits (U4, U5 or U6) are completely non-erosive and the base of the Holocene Formations could not be detected over the entire area, this base still is an indicator for the lowest expected seabed level in the considered period (2015-2046). Since the Holocene Formations are present over the entire project area (with a layer thickness between 1 and about 17m), it is very likely that morphodynamic bed level changes only occur in this layer.

Therefore, the RSBL is compared with the isopach of the base of the Bligh Bank Formation (file: SBP_Base of Bligh Bank_Formation_Unit U7.dat). For this purpose, the sample points were interpolated to the same 5x5m grid used in this study; see the left image of Figure 5.9. If the isopach is then subtracted from the measured bathymetry in 2015, the layer thickness of the Holocene Formation is obtained; see the right image of Figure 5.9.

Note that we did not use the provided sample points of the layer thickness (SBP_Thickness of Bligh Bank_Formation_Unit U7.dat) due to the low spatial resolution of these data. Since it was mentioned by Deep that the base of the Holocene Formation is “relatively planar” the adopted method of interpolating the samples of the base rather than the samples of the layer thickness yielded more accurate results.

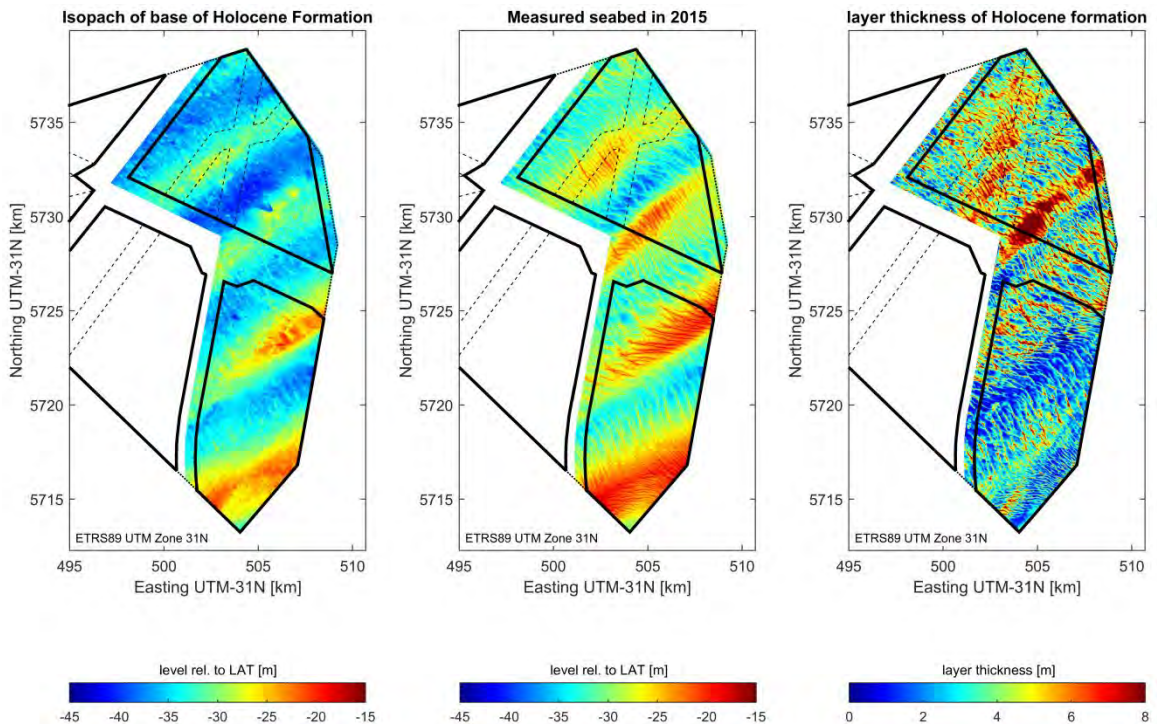


Figure 5.9 (Left) Isopach of the base of the Holocene Formation; (middle) measured seabed by multibeam survey of Deep in 2015; (right) estimated layer thickness of Holocene Formation.

The layer thickness of the Holocene Formation is then compared with the predicted maximum seabed lowering. The difference of both datasets provides an estimate for the minimum remaining layer thickness in the period 2015-2046, which is illustrated in Figure 5.10. This calculation is similar to subtracting RSBL from the base of the Holocene Formation and gave identical results for the remaining layer thickness (right image in Figure 5.10).

It can be observed that in WFS-1 only at very few locations the base of the Holocene Formation is touched or nearly touched at some time during the period of 2015-2046. In the deeper tidal channel in the middle of WFS-2, where the Holocene Formation is relatively thin more white areas can be observed, indicating that the base of the Holocene Formation is reached. The blue patch located at approximately $X = 506000$, $Y = 5723000$, indicating that the base of the Holocene Layer is penetrated by migrating sand waves is most likely not realistic, since the base of the Holocene Formation (left image in Figure 5.9) clearly shows some interpolation errors at this location, indicating that the measurements are inaccurate.

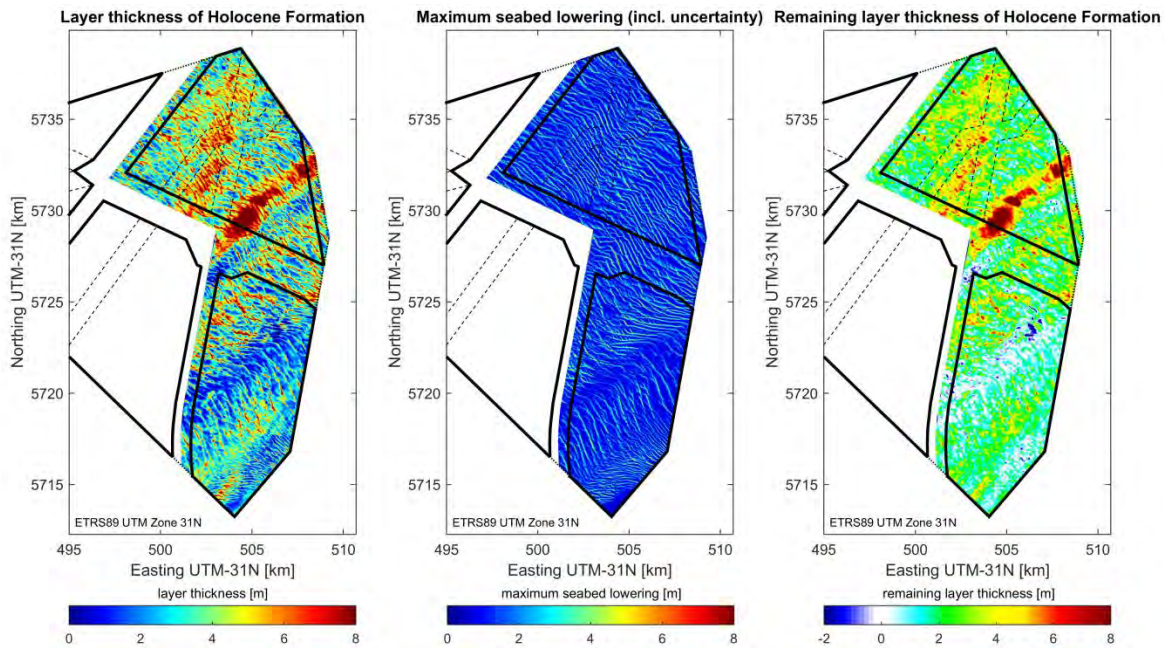


Figure 5.10 (Left) Estimated layer thickness of Holocene Formation; (middle) maximum seabed lowering including uncertainty band for period 2015-2046; (right) remaining minimum layer thickness of the Holocene Formation occurring at some time during the period 2015-2046.

It is concluded that the comparison of the RSBL with the base of the Holocene Formation shows that no unrealistic values for the seabed lowering were computed in this study. The maximum seabed lowering already resulted in small values at locations where the Holocene Formation is thin. This can be explained by the fact that sand wave amplitudes are also small at these locations. Based on these results no modifications to the RSBL were considered necessary.

5.7 Classification zones for offshore foundations and cables

In the final step, the RSBL and MSBL and the corresponding predicted seabed level lowering and rising are translated into possible classification zones for foundations and electricity cables. The classification of these zones is based on the predicted seabed level lowering or rising (see Table 5.1). The classification was chosen less strict for rising seabed levels. The reasoning behind this is that close to the structures, local scour will counteract rising seabed levels. This does not apply to the electricity cables, which are buried in the seabed; rising seabed levels can be of influence on the maximum cable temperature. Note that these classifications are for indicative and illustrational purposes only. The actual classification is dependent on the design of the support structures and properties of electricity cables and should be adjusted accordingly once this information is available.

Classification of zones	Bed level lowering [m]	Bed level rising [m]
Preferred	$0 > dz \geq -1$	$0 < dz \leq 2$
Possible	$-1 > dz \geq -2$	$2 < dz \leq 3$
Better avoided	$-2 > dz \geq -3$	$3 < dz \leq 5$
Un-recommended	$dz < -3$	$dz > 5$

Table 5.1 Classification zones.

Figure 5.11 shows how the classification zones are dependent on the RSBL, MSBL and the predicted seabed level changes. The top plot displays the location of transect 95, one of the 153 transects used in the Fourier analysis, on top of the 2015 bathymetry. The bottom plot shows the 2015 bathymetry together with the upper and lower envelope of the migrated Sand Wave Field and the RSBL and MSBL. The corresponding predicted bed level changes are displayed in the middle plot, together with the classification zones. The symmetrical shape of RSBL and MSBL indicates that the sand waves were migrated in both SE and SW direction with similar migration velocities. Furthermore, the largest seabed level changes are found respectively above and below the position of the troughs and crests in the 2015 bathymetry. For this particular transect, the predicted seabed level lowering is within the thickness of the Holocene formations (indicated by the dashed magenta line).

The spatial distribution of the classification zones is displayed in Figure 5.12. The classification of the zones differs for seabed lowering and rising (Table 5.1). This implies that for each data point, two recommendations apply; one for the predicted seabed rising and one for the predicted seabed lowering. For each point, the more strict classification of the two is displayed in the map (with 'un-recommended' being the strictest recommendation). The full overview of recommendation zones for WFS-I and WFS-II is displayed in the bottom plot of Figure 5.12. A zoom plot of the area around transect 95 is displayed in the top plot.

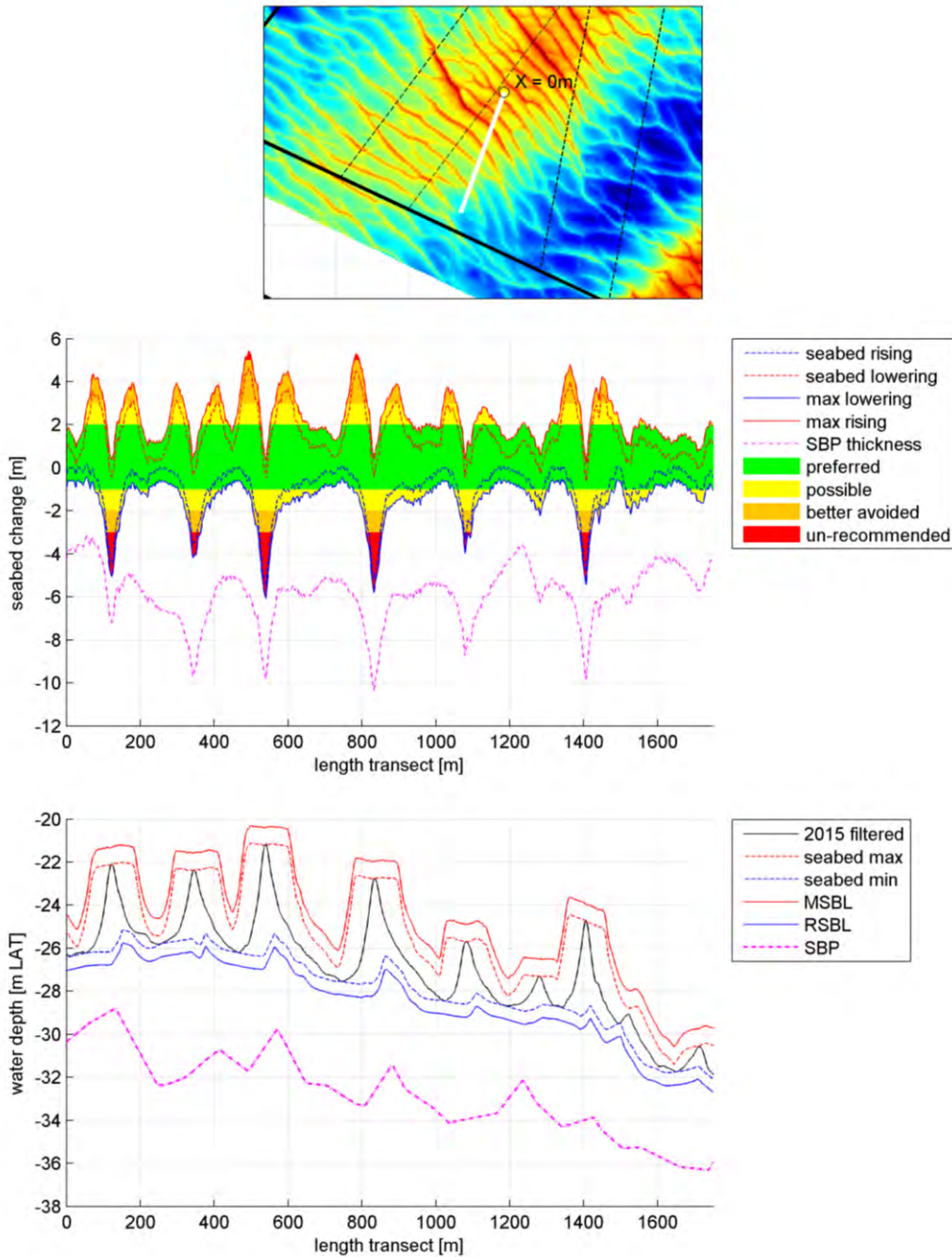


Figure 5.11 Overview of classification zones for 1 of the 153 transects (transect 95) used in the Fourier analysis. Top plot: Zoom plot of location of transect on top of the 2015 bathymetry. Middle plot: Seabed rising and lowering relative to the 2015 bathymetry (solid red/blue lines). The maximum rising and lowering, including the uncertainty bands, are indicated by the dashed red/blue lines. The thickness of the Holocene formations is indicated by the dashed magenta line. Bottom plot: 2015 bathymetry (solid black line), together with the upper envelope of the migrated Sand Wave Field (dashed red line), the lower envelope of the migrated Sand Wave Field (dashed blue line) and the RSBL (solid blue line) and MSBL (solid red line).

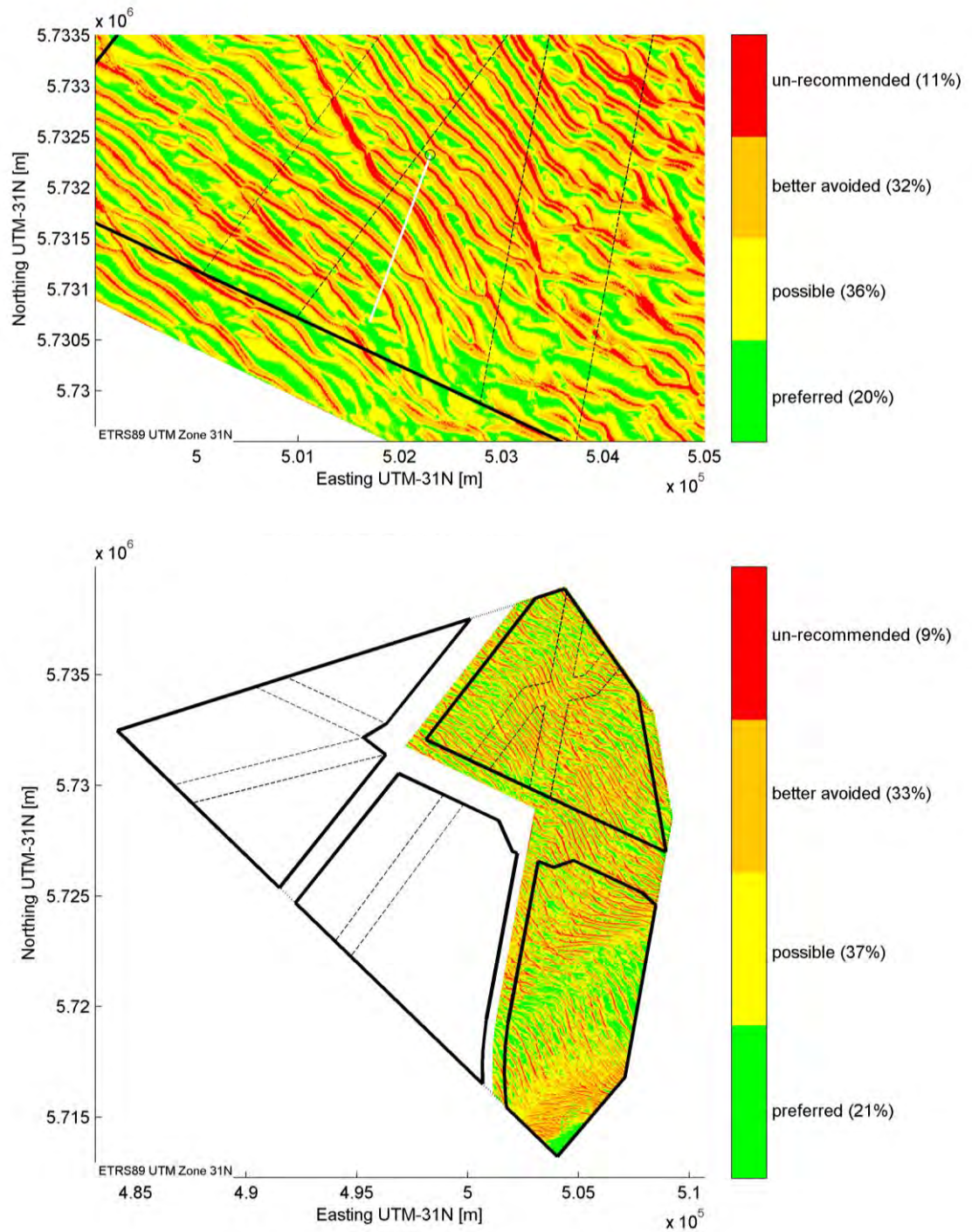


Figure 5.12 Classification zones overview maps. Top plot: Zoom plot of classification zones in area around transect 95 (see Figure 5.11). Bottom plot: Classification zones of WFS-I and WFS-II combined.

6 Conclusions and recommendations

6.1 Conclusions

The bathymetry in the Borssele Wind Farm Zone (BWFZ) consists of a complex system of shore-parallel sandbanks covered with shore-perpendicular sand waves and megaripples on top of the sand waves. A large scale bathymetrical filtering showed that the sandbanks can be considered to be static over the lifetime of the wind parks to be developed in the area. Considering the entire BWFZ, the sand waves overlying the sandbanks are mobile, have a typical average length of 230 meters, height of 4m and typical migration speeds are in the order of -1.7m/yr (north-eastern direction) to 3.2m/yr (south-western direction). The sand waves in the BWFZ show a complex behaviour, with varying (and in some locations opposing) migration directions.

The BWFZ is subdivided into four wind farm sites (WFS) for offshore wind farm development. This report deals with WFS-I and WFS-II. Table 6.1 summarizes statistics of the combined area of WFS-I and WFS-II and local sand wave characteristics per site. Although some variation in sand wave dimensions and migration speeds is observed, it is clear that significant morphodynamic activity is present in the entire BWFZ.

Area	Wave height 50% non- exceedance [m] (2010/2015)	Wavelength 50% non- exceedance [m] (2010/2015)	Migration speed 10% non- exceedance [m/yr]	Migration speed 90% non- exceedance [m/yr]
WFS-I	3.9/3.9	236/228	-1.7	1.5
WFS-II	3.2/3.3	241/242	-1.7	2.1
WFS-I and II combined	3.6/3.7	239/236	-1.7	1.9

Table 6.1 Median sand wave dimensions of WFS-I and WFS-II per individual site and combined and lower (10%) and upper (90%) estimates for the migration speeds (negative values towards northeast, positive towards southwest).

For the development of wind turbine support structures, electricity cables and high voltage stations, a Reference SeaBed Level (RSBL) and a Maximum SeaBed Level (MSBL) were obtained. These indicate, respectively, the predicted lowest and highest seabed levels in the period 2015-2046. After splitting the entire bathymetry into a Static Bathymetry (containing the underlying long-term mean bathymetry including sandbanks) and a Mobile Bathymetry (containing the Sand Wave Field and Megaripple Field), the outer envelope of the migrated Sand Wave Field was determined. The lower (mainly negative) envelope was subtracted from the Static Bathymetry to obtain the RSBL; the upper (mainly positive) envelope was added to the static bathymetry to obtain the MSBL.

The resulting RSBL shows a bathymetric shape similar to the existing static part of the bathymetry, but typically several meters lower. Comparison of the RSBL with the most recent bathymetry from 2015 shows a predicted maximum local seabed level lowering of approximately 5m. As expected, the largest lowering is found at the location of the existing sand wave crests, while minimal lowering is found at the location of the sand wave troughs. A comparison of the RSBL with the base of the Holocene Formation showed that no unrealistic values for the seabed lowering were computed in this study.

The MSBL shows a bathymetric shape similar to the existing static part of the bathymetry, but typically several meters higher. Opposite to the seabed lowering, the largest potential rise of the seabed level is found at the current locations of the troughs, with minimal rising at locations of crests. Note that the seabed close to the foundations will most likely not rise significantly, because local scour will prevent this. Buried electricity cables that cause no flow disturbance themselves will obviously not have this “beneficial” scour effect and therefore will experience a rising seabed if a sand wave crest passes over. This might be relevant for the maximum cable temperature (“thermal bottleneck effect”).

The predicted seabed level changes presented in this study follow from the applied morphological analysis techniques, describing the (uncertainty of the) physics and the natural variability of the analysed morphological system. No additional safety margins for design purposes have been applied.

6.2 Recommendations

Combined analysis of morphodynamics of WFS-I,II and WFS-III,IV

When the geophysical site investigations of WFS-III and WFS-IV are completed, it is recommended to update the processing of the entire BWFZ, including WFS-I and WFS-II. This will prevent uncertainties and inaccuracies as a result of the data processing due to, for instance, a lack of data at the boundaries. Depending on the bathymetric features outside the edges, the total range in predictions can be too small in case seabed features are migrating into the BWFZ. Also, the inner-boundary effects between WFS-I,II and WFS-III,IV are no longer present when the entire BWFZ is processed. At the outer boundaries, when data has only been collected very close to the boundaries of the sites, this will still be a problem. Potentially, the area within 50m of the 2015-survey boundaries is affected and, as a consequence, the RSBL and MSBL may be less reliable. This can however artificially be solved by substituting with high resolution 2010 data outside the 2015 measured boundaries and accounting for the different survey times of the data in the calculation of the bed level changes.

Numerical modelling of hydrodynamics

In order to better understand the morphodynamic activity in the area and to be able to further narrow down the vertical range in seabed predictions (difference between MSBL and RSBL), it is recommended to set up a detailed hydrodynamic model of the area and simulate the tidal currents. Sand wave behaviour is governed by the currents (most prominently by asymmetries in a tidal cycle). By numerical modelling of at least one representative spring-neap cycle at a high spatial and temporal resolution a valuable dataset of velocity patterns is generated. The results should be outputted in map fields of the Borssele wind farm zone, with a temporal resolution of approximately 10 minutes and a spatial resolution of maximum 50m. These results can be used to accurately determine relatively small net changes in sediment transport rates and directions over the sandbanks, responsible for the variation in sand wave characteristics. Especially in areas where the calculation of the migration direction for the different considered survey periods (2000-2010, 2000-2015 and 2010-2015) showed large variation, numerical modelling may provide more accurate understanding of the actual migration direction.

Please note that these model results are not only useful to further validate the results for this second phase of the study, but also for future in-depth studies (e.g. regarding scour) at the locations of the turbine foundations and electricity cables. Note that it is not proposed to use this model for morphological simulations: for such a large area such simulations would be very computationally expensive (too time-consuming).

References

Ashley, G.M. (1990). Classification of large-scale subaqueous bedforms: a new look on an old problem. *Journal of Sedimentary Petrology* **60**(1): 160-172.

Besio, G., P. Blondeaux, M. Brocchini and G. Vittori (2004). On the modeling of sand wave migration. *Journal of Geophysical Research* **109**(C04018).

Besio, G., Blondeaux, P., Vittori, G., 2006. On the formation of sand waves and sand banks. *Journal of Fluid Mechanics* 557, 1-27.

Borsje, B.W., De Vries, M.B., Bouma, T.J., Besio, G., Hulscher, S.J.M.H., Herman, P.M.J., 2009. Modelling bio-geomorphological influences for offshore sandwaves. *Continental Shelf Research* 29, 1289-1301.

Borsje, B.W., W.M. Kranenburg, P. C. Roos, J. Matthieu, S.J.M.H. Hulscher, 2014. The role of suspended load transport in the occurrence of tidal sand waves. *J. Geophys. Res.* 119:1-16.

Buijsman, M.C. and H. Ridderinkhof (2008a). Long-term evolution of sand waves in the Marsdiep inlet, II: relation to hydrodynamics. *Continental Shelf Research* **28**(9): 1202-1215.

Buijsman, M.C. and H. Ridderinkhof (2008b). Long term evolution of sand waves in the Marsdiep inlet, I: high-resolution observations. *Continental Shelf Research* **28**(9): 1190-1201.

Cherlet, J., Besio, G., Blondeaux, P. van Lancker, V., Verfaillie, E., Vittori, G., 2007. Modeling sand wave characteristics on the Belgian Continental Shelf and in the Calais-Dover Strait. *Journal of Geophysical Research*, Vol. 112, C06002, doi:10.1029/2007/JC004089.

Crux Engineering BV (2014), Windpark Borssele Geological desk study.

Deep (2015a), Site Studies Wind Farm Zone Borssele - Geophysical survey wind farm site I. 20150403_SDB_DEEP_Final report WFS1_V02_F.docx, P2849, final report dated 3 April 2015.

Deep (2015b), Site Studies Wind Farm Zone Borssele - Geophysical survey wind farm site II. 20150403_SDB_DEEP_Final report WFS2_V02_F.docx, P2849, final report dated 3 April 2015.

Deltares (2008), Sand wave dynamics Bligh Bank. Report H5239.

Deltares (2011), The scientific validation of the hydrographic survey policy of the Netherlands Hydrographic Office, Royal Netherlands Navy. Ref: 1201907-000-BGS-0008.

Deltares (2014), Site Studies Wind Farm Zone Borssele - Morphodynamics of Borssele Wind Farm Zone; prediction of potential seabed level changes during the lifetime of offshore wind parks. Ref: 1210520-000-HYE-0002; draft report v2.0, dated 23 December 2014.

Dorst, L.L., Roos, P.C., Hulscher S.J.M.H., Lindenbergh, R.C., (2009). The estimation of sea floor dynamics from bathymetric surveys of a sand wave area. *Journal of Applied Geodesy* 3(3), 97-120.

Dorst, L.L., P.C. Roos and S.J.M.H. Hulscher (2011). Spatial differences in sand wave dynamics between the Amsterdam and the Rotterdam region in the Southern North Sea. *Continental Shelf Research* 31: 1096-1105.

Houthuys, R., A. Trentesaux and P. De Wolf (1994). Storm influences on a tidal sandbank's surface (Middelkerke Bank, southern North Sea). *Marine Geology* 121: 23-41.

Hulscher, S.J.M.H. (1996). Tidal-induced large-scale regular bed form patterns in a three-dimensional shallow water model. *Journal of Geophysical Research* 101(C9): 20,727-720,744.

Hulscher, S.J.M.H., Van den Brink, G.M. (2001). Comparison between predicted and observed sand waves and sand banks in the North Sea. *Journal of Geophysical Research* C5, 106, 9327-9338.

IHO. (1988), IHO Standards for Hydrographic Surveys, Special publication 44, 4th ed. Monaco: International Hydrographic Bureau.

Knaapen, M.A.F. (2005). Sandwave migration predictor based on shape information *Journal of Geophysical Research* 110(F04S11): 9.

Knaapen, M.A.F., Hulscher, S.J.M.H., (2002). Regeneration of sand waves after dredging. *Coastal Engineering* 46, 277-289.

Matthieu, J., Raaijmakers, T.C. (2012). Interaction between offshore pipelines and migrating sand waves. Proceedings of the 31st International Conference on Ocean, Offshore and Arctic Engineering, OMAE 2012, 10-15 June 2012, Rio de Janeiro, Brazil

McCave, I.N., (1971). Sand waves in the North Sea off the coast of Holland. *Marine Geology* 10, 199-225.

Németh, A.A., Hulscher, S.J.M.H., De Vriend, H.J., (2002). Modelling sand wave migration in shallow shelf seas. *Continental Shelf Research* 22, 2795–2806.

Papilli, S., T. Wever, Y. Dupont and V. Van Lancker (2014). Storm influence on the burial of objects in a shallow sandy shelf environment. *Marine Geology* 349: 61-72.

Passchier, S. and M.G. Kleinhans (2005). Observations of sand waves, megaripples and hummocks in the Dutch coastal area and their relation to currents and combined flow conditions. *Journal of Geophysical Research* 110(F04S15).

Peters, S.E. and D.P. Loss (2012). Storm and fair-weather wave base: a relevant distinction? *Geology* 40(6): 511-514.

Rijkswaterstaat (2014), Windenergiegebied Borssele Concept-kavelindeling.pdf

Sterlini, F.M. (2009). *Modelling sand wave variation*. Department of Water Engineering and Management. Enschede, University of Twente, Netherlands. **Ph.D.**

Sterlini, F.M., S.J.M.H. Hulscher and D.M. Hanes (2009). Simulating and understanding sand wave variation: a case study of the Golden Gates sand waves. . *Journal of Geophysical Research* **114**(F02007).

Sterlini, F.M., T.A.G.P. Van Dijk, S. IJzer and S.J.M.H. Hulscher (2012). *Seasonal changing sand waves and the effect of surface waves*. 5th International Short Conference on Applied Coastal Research (SCACR 2011), Aachen, Germany,

Terwindt, J.H.J. (1971). Sand waves in the Southern Bight of the North Sea. *Marine Geology* **10**: 51-67.

Van Alphen, J.S.L.J., Damoiseaux, M.A. (1989), A geomorphological map of the Dutch shoreface and adjacent part of the continental shelf. *Geologie en Mijnbouw* 68(4): 433-443.

Van Dijk, T.A.G.P. and M.G. Kleinhans (2005). Processes controlling the dynamics of compound sand waves in the North Sea, Netherlands. *Journal of Geophysical Research* **110**(F04S10).

Van Dijk, T.A.G.P. and P.J.P. Egberts (2008). *The variability of sand wave migration in the North Sea*. 3rd International Workshop on Marine and river dune dynamics (MARID2008), University of Leeds, Leeds, UK,

Van Dijk, T.A.G.P., Lindenbergh, R.C., Egberts, P.J.P. (2008), Separating bathymetric data representing multiscale rhythmic bed forms: A geostatistical and spectral method compared. *Journal of geophysical research* 113.

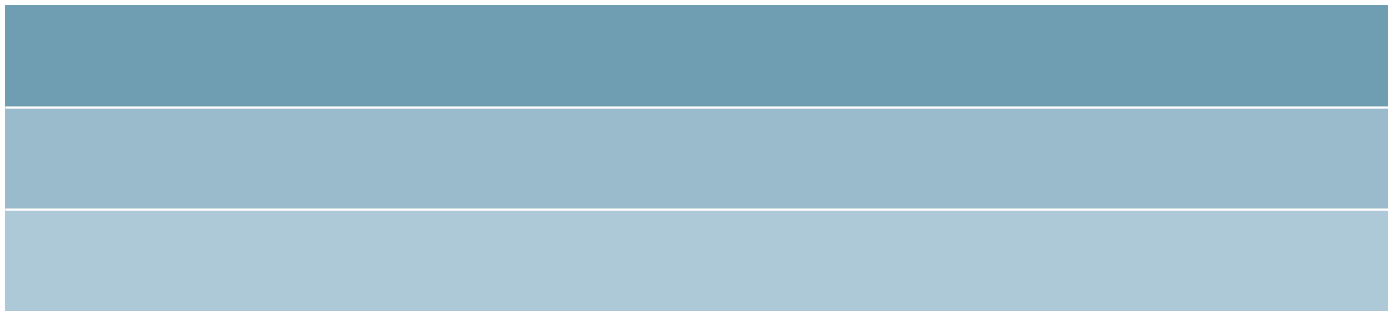
Van Dijk, T.A.G.P., C. Van der Tak, W.P. De Boer, M.H.P. Kleuskens, P.J. Doornenbal, R.P. Noorlandt and V.C. Marges (2011). *The scientific validation of the hydrographic survey policy of the Netherlands Hydrographic Office, Royal Netherlands Navy*. Deltares, Report 1201907-000-BGS-0008: 165 pp, <http://kennisonline.deltares.nl/3/m/search/products.html?q=hydrographic&qtype=1>.

Van Lancker, V., Houziaux, Baeye, J.S, Van den Eynde, M. D., Rabaut M., Troost, K., Vermaas, T., Van Dijk T.A.G.P. (2013), Biogeomorphology in the field: bedforms and species, a mystic relationship. Proceedings of MARID 2013: Fourth International Conference on Marine and River Dune Dynamics. Bruges, Belgium, 15-17 April 2013.

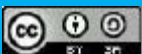
Van Santen, R.B., H.E. De Swart and T.A.G.P. Van Dijk (2011). Sensitivity of tidal sand wavelength to environmental parameters: A combined data analysis and modelling approach. *Continental Shelf Research* **31**(9): 966-978.

Wiertsema & Partners (2008), Long term stability analysis Bligh Bank.

Yalin, M.S. (1964), Geometrical properties of sand waves. *J. Hydraul. Div., ASCE*, 90, 105–19.



Deltares



The creative commons license 4.0 apply to this material.

This investigation was carried out by Deltares, commissioned by RVO.nl, an agency of the Ministry of Economic Affairs. Whilst a great deal of care has been taken in compiling the contents of this investigation, RVO.nl can not be held liable for any damages resulting from any inaccuracies and/or outdated information.

Contacts

Netherlands Enterprise Agency (RVO.nl)
Croeselaan 15 | 3521 BJ | Utrecht
P.O. Box 8242 | 3503 RE | Utrecht
www.rvo.nl / <http://english.rvo.nl>

Netherlands Enterprise Agency (RVO.nl) | July 2015